

# Reservoir Computing via Quantum Recurrent Neural Networks

Samuel Yen-Chi Chen,<sup>1</sup> Daniel Fry,<sup>2</sup> Amol Deshmukh,<sup>2</sup>

Vladimir Rastunkov,<sup>2</sup> and Charlee Stefanski<sup>1</sup>

<sup>1</sup>*Wells Fargo*

<sup>2</sup>*IBM Quantum, IBM Research*

(Dated: November 7, 2022)

## Abstract

Recent developments in quantum computing and machine learning have propelled the interdisciplinary study of quantum machine learning. Sequential modeling is an important task with high scientific and commercial value. Existing VQC or QNN-based methods require significant computational resources to perform the gradient-based optimization of a larger number of quantum circuit parameters. The major drawback is that such quantum gradient calculation requires a large amount of circuit evaluation, posing challenges in current near-term quantum hardware and simulation software. In this work, we approach sequential modeling by applying a reservoir computing (RC) framework to quantum recurrent neural networks (QRNN-RC) that are based on classical RNN, LSTM and GRU. The main idea to this RC approach is that the QRNN with randomly initialized weights is treated as a dynamical system and only the final classical linear layer is trained. Our numerical simulations show that the QRNN-RC can reach results comparable to fully trained QRNN models for several function approximation and time series prediction tasks. Since the QRNN training complexity is significantly reduced, the proposed model trains notably faster. In this work we also compare to corresponding classical RNN-based RC implementations and show that the quantum version learns faster by requiring fewer training epochs in most cases. Our results demonstrate a new possibility to utilize quantum neural network for sequential modeling with greater quantum hardware efficiency, an important design consideration for noisy intermediate-scale quantum (NISQ) computers.

## I. INTRODUCTION

Quantum computing (QC) has been demonstrated theoretically to provide significant speedup over classical computers in several computational tasks [1, 2]. Notable examples include the factoring of large numbers [3] and searching an unstructured database [4]. Recent advances in quantum hardware by companies such as IBM [5], Google [6] and IonQ [7] provide enable the opportunity to implement quantum algorithms on real devices. At the same time, the development of various machine learning (ML) techniques has accelerated progress in fields such as natural language processing [8, 9], automatic speech recognition [10–13], computer vision [14–18], complex sequential decision making [19–23] and many more.

Considering the ever increasing data volume and complexity of accessible data, it is reasonable to examine whether we can build more powerful ML methods with the help of a novel computing paradigm. QC is a leading candidate and the attempt to address this problem led to the development of quantum machine learning (QML) [24, 25]. Sequential modeling is a common ML task and has been studied extensively in the classical setting. For example, the recurrent neural network (RNN) [26–28] and its variants—such as gated recurrent units (GRU) [29] and long short-term memory (LSTM) [30]—has a long history of being applied in machine translation [8, 9], speech recognition [10–13] and time-series analysis [31, 32], just name a few. Indeed, sequential modeling has also been studied in the QML field via the use of quantum recurrent networks (QRNN) [33, 34] and its variants such as quantum long short-term memory (QLSTM) [35]. However, existing methods using QRNN and its variants to study sequential modeling suffers from a major drawback: long training time. QML methods for sequential modeling such as QRNN and QLSTM largely depend on the iterative optimization of quantum circuit parameters. Notable examples are variational quantum algorithms (VQA) [36] and quantum circuit learning (QCL) [37]; both require a significant amount of circuit evaluation to calculate the gradients and update the circuit parameters [38]. For example, the commonly used *parameter-shift* quantum gradient calculation method requires two circuit evaluations for each parameter [37, 38].

Intuitively, one can ask the following question: can we only train part of the model instead of all of the parameters and achieve comparable results? The answer is yes when classical RNNs are randomly initialized to process the sequence and only the final linear layer is trained. Such architecture is called *reservoir computing* (RC) [39–41]. While RC based

on classical RNN has demonstrated significant success, as described in [39, 40], it is not yet clear whether their quantum counterpart (e.g. quantum RNN and variants) can achieve comparable or superior results. In this paper, we propose a reservoir computing (RC) method based on randomly initialized quantum circuits. Specifically, we investigate the quantum version of RNN-based RC. We consider the following quantum RNN: quantum recurrent neural network (QRNN), quantum long short-term memory (QLSTM) and a quantum gated recurrent unit (QGRU). We apply the untrained QRNN, QGRU and QLSTM as the reservoir and only train the final classical linear layer which is used to process the output from the respective quantum reservoirs.

The numerical simulations show that the QRNN-RC can reach results comparable to fully trained QRNN models in several function approximation and time-series prediction tasks. Since the QRNNs in the proposed model does not need to be trained, the overall process is much faster than the fully trained ones. We also compare to classical RNN-based RC and show that in most cases the quantum version learns faster or requires fewer training epochs.

The paper is organized as follows: In Section II the basic notion of reservoir computing is described. In Section III we introduce the VQC which is the building block of QML models. We describe various kinds of QRNNs in the Section IV. The experimental settings are described in Section V and the results are shown in Section VI. Finally, we discuss the results in Section VII and provide concluding remarks in Section VIII.

## II. RESERVOIR COMPUTING

A fundamental task in machine learning is to model temporal or sequential data. Examples of this include ML models trained to process audio or text data to perform natural language processing [8–13], or analyze financial data to provide better decision making [42, 43]. Various recurrent neural networks (RNN) are often used to achieve these tasks. However, there are challenges when training RNN such as vanishing or exploding gradients [44, 45], and training RNNs is usually computationally expensive.

Reservoir computing (RC) is defined in [46] as an approach to processing sequential data, where large, nonlinear, randomly connected, and fixed recurrent network (the *reservoir*) is separated from a linear output layer with trainable parameters. It is assumed that the complexity of the recurrent network allows one to learn the desired output by using only

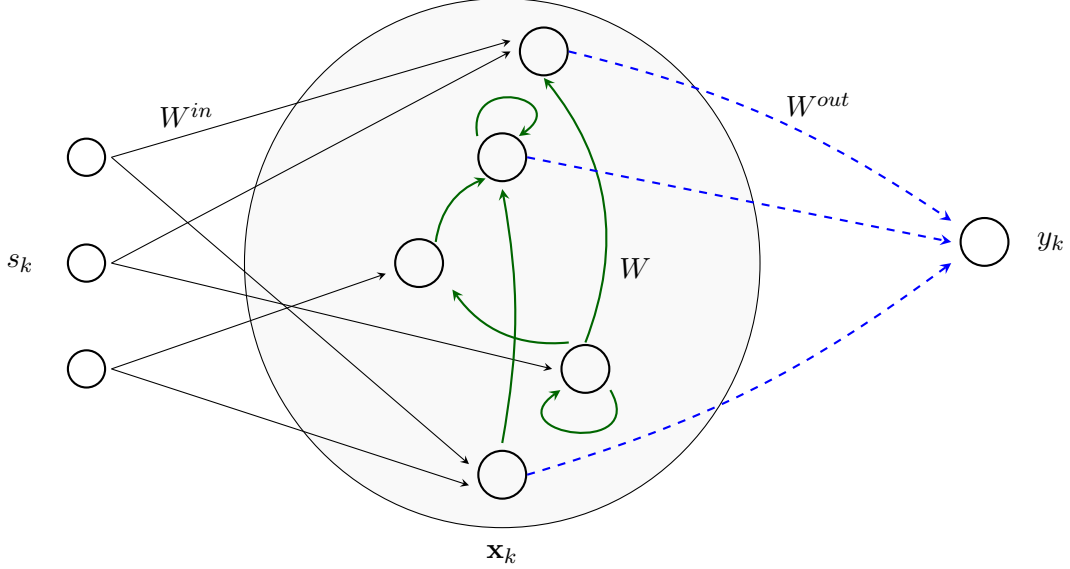


FIG. 1. **Reservoir computing (RC).**

a linear combination of its activations [39]. The linear output layer is fast to train, so it helps to mitigate issues with RNN training discussed above. RC based on RNN, as depicted in Figure 1, is sometimes referred to as the echo state network [40]. It can be summarized mathematically as follows:

$$\begin{aligned} \mathbf{x}_k &= \mathbf{f}(W^{in} s_k + W \mathbf{x}_{k-1}) \\ y_k &= W^{out} \mathbf{x}_k^{out}, \end{aligned} \quad (1)$$

where  $s_k$  and  $x_k$  correspond to the input signal, and state of the reservoir, respectively, at step  $k$ . Here,  $W$ ,  $W^{in}$ , and  $W^{out}$  correspond to the internal weights of the reservoir, the weights connecting the input nodes to the nodes in the reservoir, and the weights connecting the reservoir nodes to the output nodes, respectively. Only  $W^{out}$  needs to be trained, other weights are randomly initialized.

With the success of classical RNN-based reservoirs, it is natural to consider a similar idea in the quantum regime. Specifically, we consider the quantum version of common RNN architectures such as quantum RNN, quantum long short-term memory (QLSTM) and quantum gated recurrent unit (QGRU). Along with the idea of classical RNN-based RC, we replaced the classical neural networks inside these RNN architectures with variational quantum circuits (VQC) which have been shown to have certain advantages over classical

neural networks [47–49]. In the next section, we will describe the building blocks of these quantum RNNs.

### III. VARIATIONAL QUANTUM CIRCUITS

A variational quantum circuit (VQC) (also known as a parameterized quantum circuit (PQC)), is a quantum circuit which depends on tunable parameters. The parameters can be tuned via gradient-based [38, 50] or gradient-free algorithms [50, 51]. Figure 2 illustrates a generic VQC which consists of three parts: state preparation, the parameterized circuit, followed by measurement. In the figure,  $U(\mathbf{x})$  represents the state preparation circuit which encodes classical data  $\mathbf{x}$  into a quantum state.  $V(\boldsymbol{\theta})$  represents the variational or parameterized circuit with *learnable* or adjustable parameters  $\boldsymbol{\theta}$ , which, in the context of this paper, is optimized using gradient-descent. The output is obtained as a classical bit string through measurement of a subset (or all) of the qubits.

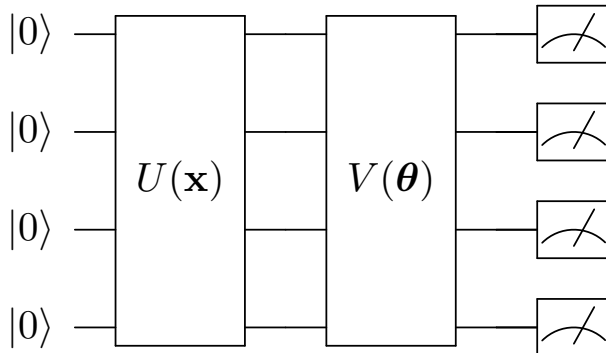


FIG. 2. **Generic architecture for variational quantum circuits (VQC).**  $U(\mathbf{x})$  is a quantum circuit for encoding the classical input data  $\mathbf{x}$  into a quantum state and  $V(\boldsymbol{\theta})$  is the variational circuit with tunable or learnable parameters  $\boldsymbol{\theta}$  which is optimized via gradient-based or gradient-free methods. This circuit is followed by measurement of some or all of the qubits.

Noteworthy advantages of VQCs include resilience of quantum noise [52–54], which makes them favorable for NISQ era quantum devices, and the ability to train VQCs with smaller datasets [47]. Quantum machine learning methods using VQCs demonstrate a varying degree of success. Notable examples VQC applications include function approximation [35, 37], classification [37, 55–75], generative modeling [76–80], deep reinforcement learning [81–94], sequence modeling [33–35], speech recognition [95, 96], natural language processing [97, 98],

metric and embedding learning [99, 100], transfer learning [59] and federated learning [95, 101, 102]. Additionally, it has been shown that the VQCs may have more expressive power than classical neural networks [48, 49, 103, 104]. The *expressive power* is defined by the ability to represent certain functions or distributions given a limited number of parameters or a specified model size. Indeed, artificial neural networks (ANNs) are known as *universal approximators* [105], i.e. a neural network with even one single hidden layer can, in principle, approximate any computable function. However, as the complexity of the function grows, the number of neurons required in the hidden layer(s) may become extremely large, increasing the demand for computational resources. Thus, it is worthwhile to examine whether VQCs can perform better than their classical counterparts with an equally limited number of parameters.

In the optimization procedure, we employ the *parameter-shift* method to derive the analytical gradient of the quantum circuits, as described in [38, 106]. In this paper, VQCs are operated in the following ways: (i) in the reservoir computing cases, the VQCs are randomly initialized and then the parameters are fixed, no quantum gradients are needed in this case. (ii) In the full optimization cases, the VQCs are optimized through gradient-based methods. In the next section, we describe the quantum version of RNNs used in this work.

#### IV. QUANTUM RECURRENT NEURAL NETWORK

RNNs are a special kind of ML model designed to handle sequential modeling via the memory capabilities which can keep track of previous information. What makes RNNs and its variants special is that the output from the RNN will be fed into the model again to retain previous information. The value fed back to the RNN is called the *hidden* state. This is the major difference between a RNN and a fully-connected neural network. RNNs can be used to learn and output a whole sequence or predict a single value. In the first case, at each time step  $t$ , given the hidden state from the previous time  $h_{t-1}$  and the input  $x_t$ , the RNN will output the prediction  $y_t$  and the hidden state  $h_t$ . In the other case, if we choose to use the RNN to predict a single value, then given an input sequence  $\{x_0, x_1, \dots, x_n\}$ , only the final  $y_n$  will be retained.

The generic form of a RNN suffers from several challenges such as vanishing gradients [44, 45] and failing to learn long-range temporal dependencies [44, 45]. Various modified forms of

RNNs have been proposed to fix these issues such as long short-term memory (LSTM) [30] and gated recurrent units (GRU) [29], which have demonstrated superior performance over the generic RNN in a wide range of applications [107]. RNN and its variants such as LSTM and GRU can be used to serve as a high-dimensional dynamical system or as a *reservoir*. In this case, the RNN is not trained, meaning that its parameters are fixed after the random initialization [108]. The only trainable part is the final linear layer which will process the output from the RNN.

### A. Quantum Recurrent Neural Network

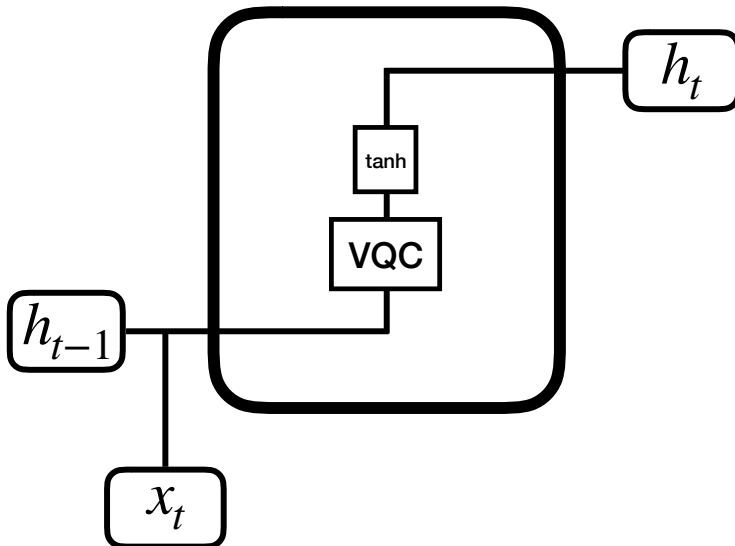


FIG. 3. The quantum recurrent neural networks (QRNN) architecture.

The quantum recurrent neural network (QRNN) is the quantum version of the conventional RNN. The major distinction is that the classical neural network is replaced by a VQC, as shown in Figure 3. The formulation of a QRNN cell is given by

$$h_t = \tanh(VQC(v_t)) \quad (2a)$$

$$y_t = NN(h_t) \quad (2b)$$

where the input is the concatenation  $v_t$  of the hidden state  $h_{t-1}$  from the previous time step and the current input vector  $x_t$ . The VQC is detailed in the Section IV D. In this work,  $x_t$

is set to be one-dimensional and the hidden unit  $h_t$  is set to be three-dimensional. Since the model is built to generate the prediction of a scalar value, the output from the QRNN,  $h_t$ , at the last time step (in the context of this paper the last step is  $t = 4$ ) will be processed by a classical neural network layer  $NN$  (as in Equation 2b).

## B. Quantum Long Short-term Memory

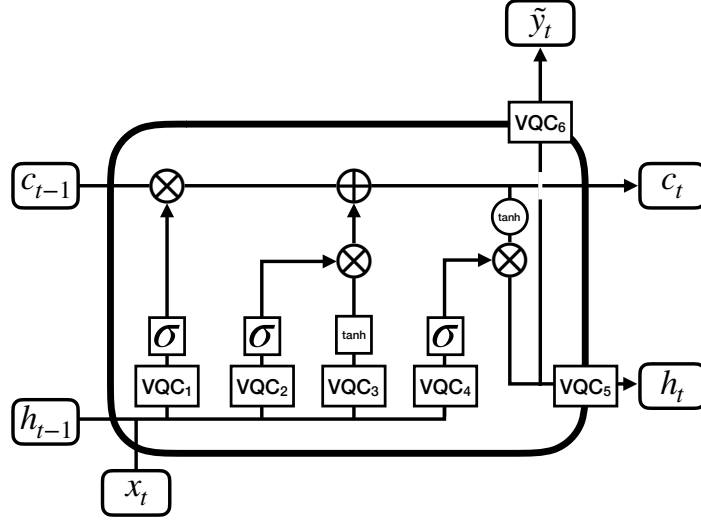


FIG. 4. The quantum long short-term memory (QLSTM) architecture.

The quantum long short-term memory (QLSTM) [35] is an improved version of QRNN. There are two memory components in a QLSTM, namely the hidden state  $h_t$  and the cell or internal state  $c_t$ . A formal mathematical formulation of a QLSTM cell is given by

$$f_t = \sigma(VQC_1(v_t)) \quad (3a)$$

$$i_t = \sigma(VQC_2(v_t)) \quad (3b)$$

$$\tilde{C}_t = \tanh(VQC_3(v_t)) \quad (3c)$$

$$c_t = f_t * c_{t-1} + i_t * \tilde{C}_t \quad (3d)$$

$$o_t = \sigma(VQC_4(v_t)) \quad (3e)$$

$$h_t = VQC_5(o_t * \tanh(c_t)) \quad (3f)$$

$$\tilde{y}_t = VQC_6(o_t * \tanh(c_t)), \quad (3g)$$

$$y_t = NN(\tilde{y}_t) \quad (3h)$$

where the input is the concatenation  $v_t$  of the hidden state  $h_{t-1}$  from the previous time step and the current input vector  $x_t$ . The VQC is detailed in the Section IV D. In this work, the  $x_t$  is set to be one dimensional and the hidden unit  $h_t$  is set to be three dimensional. The cell state or internal state  $c_t$  is set to be four-dimensional. Since the model is built to generate the prediction of a scalar value, the output from the QLSTM  $\tilde{y}_t$  at the last time step (in the context of this paper the last step is  $t = 4$ ) will be processed by a classical neural network layer  $NN$  to get  $y_t$ .

### C. Quantum Gated Recurrent Unit

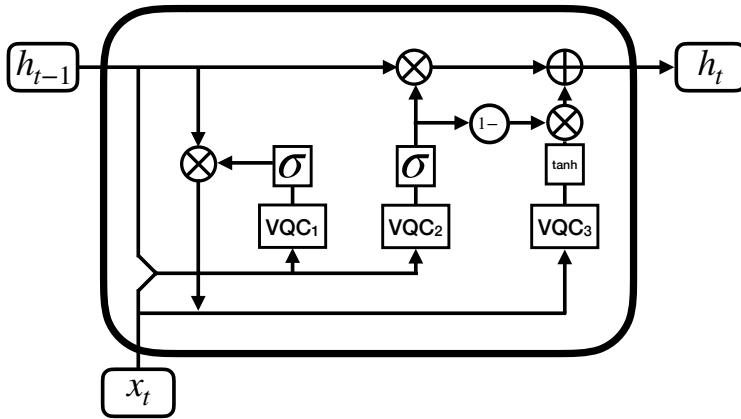


FIG. 5. The quantum gated recurrent units (QGRU) architecture.

The quantum gated recurrent unit (QGRU) is another QRNN with gating mechanisms similar to QLSTM. QGRU has fewer parameters and simpler architectures than QLSTM. A formal mathematical formulation of a QGRU cell is given by

$$r_t = \sigma(VQC_1(v_t)) \quad (4a)$$

$$z_t = \sigma(VQC_2(v_t)) \quad (4b)$$

$$o_t = \text{cat}(x_t, r_t * H_{t-1}) \quad (4c)$$

$$\tilde{H}_t = \tanh(VQC_3(o_t)) \quad (4d)$$

$$H_t = z_t * H_{t-1} + (1 - z_t) * \tilde{H}_t \quad (4e)$$

$$y_t = NN(H_t) \quad (4f)$$

where the input is the concatenation  $v_t$  of the hidden state  $H_{t-1}$  from the previous time

step and the current input vector  $x_t$ . The VQC is detailed in the Section IV D. In this work, the  $x_t$  is set to be one-dimensional and the hidden unit  $H_t$  is set to be three-dimensional. Since the model is built to generate the prediction of a scalar value, the output from the QGRU  $H_t$  at the last time step (in the context of this paper the last step is  $t = 4$ ) will be processed by a classical neural network layer  $NN$  to get  $y_t$ .

#### D. VQC Components

The specific VQC components used in this paper are represented in Figure 6. As previously mentioned, a VQC includes the following three parts: an *encoding circuit*, a *variational circuit* and *quantum measurement*.

##### 1. Encoding Circuit

A quantum state with  $N$ -qubits can be defined as

$$|\psi\rangle = \sum_{(q_1, q_2, \dots, q_N) \in \{0,1\}} c_{q_1, q_2, \dots, q_N} |q_1\rangle \otimes |q_2\rangle \otimes \dots \otimes |q_N\rangle, \quad (5)$$

where  $c_{q_1, \dots, q_N} \in \mathbb{C}$  is the complex *amplitude* for each basis state and  $q_i \in \{0,1\}$ . The square of the amplitude  $c_{q_1, \dots, q_N}$  is the measurement *probability* for the corresponding value in  $|q_1\rangle \otimes |q_2\rangle \otimes \dots \otimes |q_N\rangle$ , such that the total probability is 1:

$$\sum_{(q_1, \dots, q_N) \in \{0,1\}} ||c_{q_1, \dots, q_N}||^2 = 1. \quad (6)$$

The encoding circuit maps classical data values to quantum amplitudes. In this paper, we use the encoding procedure described in [35]. The circuit is initialized in the ground state and then Hadamard gates are applied to create an unbiased initial state. We use a two-angle encoding, similar to dense angle encoding [109], but for encoding one value with two angles. This involves encoding each data value to a qubit with a series of two gates,  $R_y$  and  $R_z$ , respectively. The angles of the rotation gates are given by  $f(x_i) = \arctan(x_i)$  and  $g(x_i) = \arctan(x_i^2)$ , respectively, where  $x_i$  is a component of data vector  $\mathbf{x}$ . The quantum state of the encoded data takes the form

$$|\mathbf{x}\rangle = \bigotimes_{i=1}^N \cos\left(f(x_i) + \frac{\pi}{4}\right) |0\rangle + \exp(ig(x_i)) \sin\left(f(x_i) + \frac{\pi}{4}\right) |1\rangle \quad (7)$$

where  $N$  is the dimensionality of  $\mathbf{x}$  and the  $\pi/4$  angle offset accounts for the initial Hadamard rotations.

## 2. Variational Circuit

The trainable (or learnable) part of the VQC is the *variational* circuit. This is a parameterized circuit where the parameters are subject to iterative optimization, such as gradient-descent. In this paper, the variational part includes several *blocks*, represented as dashed boxes in Figure 6. Each block consists of multiple CNOT gates to entangle qubits, and unitary rotation gates controlled by learnable parameters  $\alpha$ ,  $\beta$  and  $\gamma$ . The blocks can be repeated several times to increase the number of parameters.

## 3. Quantum Measurement

Our hybrid quantum-classical architecture relies on the ability to move data between quantum and classical systems. To extract the information from the quantum circuit, we perform quantum measurements. Consider the circuit shown in Figure 6 as an example, if we run the circuit once, we will get a bit string like 0011 since we measure all the four qubits. Due to the probabilistic nature of quantum systems, we will get different bit strings at each circuit repetition and measurement. In the next run, it may be, for example, 0110. If we run the circuit many times (number of *shots*), we can get a distribution of the measurement results, called the *expectation values* of the observable. The expectation values can be calculated analytically when using a quantum simulator software without noise, or multiple sampling when a certain device noise model is specified. Given an operator  $\hat{O}$ , the expected value for a state  $|\psi\rangle$  is given by

$$\mathbb{E}[\hat{O}] = \langle\psi|\hat{O}|\psi\rangle. \quad (8)$$

In our case,  $|\psi\rangle$  corresponds to the state  $U|\mathbf{x}\rangle$  in which  $|\mathbf{x}\rangle$  is the encoded data vector as defined in Equation 7, and  $U$  is the variational circuit.

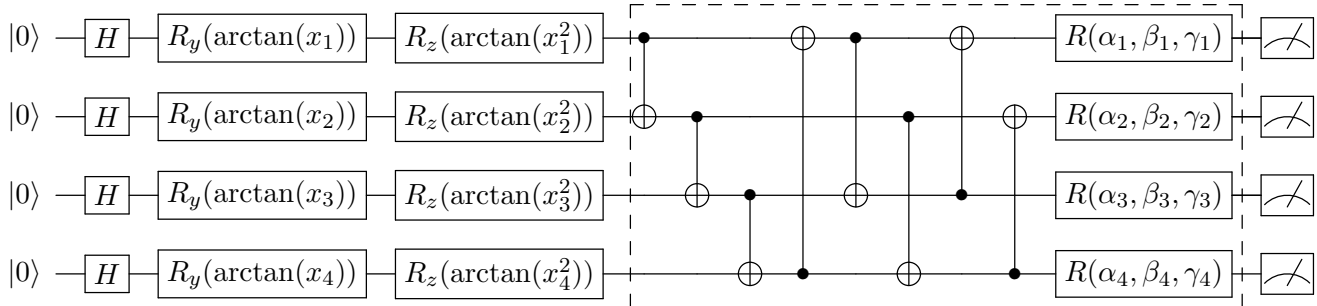


FIG. 6. **Generic VQC architecture for QRNN, QLSTM and QGRU.** The VQC we use for QRNN, QLSTM and QGRU includes the following three parts: the data encoding circuit (with  $H$ ,  $R_y$ , and  $R_z$  gates), the variational or parameterized circuit (shown within the dashed outline), and the measurement. Note that the number of qubits and the number of measurements can be adjusted to fit the problem of interest (various input and output dimensions), and the variational layer can contain several iterations to increase the model size or the number of parameters, depending on the capacity and capability of the quantum machine or quantum simulation software used for the (actual or numerical) experiments. In the context of this paper, the number of qubits used is 4.

## V. NUMERICAL EXPERIMENTS

We compare the performance of full optimization and reservoir computing as well as the effect of quantum device noise. In the optimization procedure of quantum circuits, we employ the *parameter-shift* method to derive the analytical gradient of quantum parameters. The method is described in [38, 106]. Additionally, we compare our quantum models to classical models with a similar number of parameters. We present the learning performance of these models at different numbers of training epochs. For a better comparison with previous works, the experimental setting follows that in [35]. We reproduce similar results of fully trained QLSTM and apply the same procedure to QRNN and QGRU. We use PyTorch [110] for the overall ML workflow, PennyLane [106] for building the quantum circuits and Qiskit [5] for noisy quantum simulation.

The training and testing scheme follows that in [35]. Concisely, the model is expected to predict the  $(N + 1)$ -th value given the first  $N$  values in the sequence. For function approximation tasks (described in Section V E 1 and Section V E 2), at step  $t$  if the input is  $[x_{t-4}, x_{t-3}, x_{t-2}, x_{t-1}]$  (i.e.,  $N = 4$ ), then the model is expected to generate the output  $y_t$ , which should be close to the ground truth  $x_t$ . For time series prediction tasks (described in

Section V E 3), at step  $t$ , if the input is  $[u_{t-4}, u_{t-3}, u_{t-2}, u_{t-1}]$  (i.e.,  $N = 4$ ) from the *input sequence*, then the model is expected to generate the output  $y_t$ , which should be close to the ground truth  $v_t$  in the *target sequence*. We set  $N = 4$  for all experiments in this paper.

### A. Full Optimization

In this part, we present the full optimization (e.g. training all the quantum parameters) of the QRNN to be referenced as the baseline. We consider the QRNN, QGRU and QLSTM models with the following model configurations: For function approximation tasks such as damped SHM and Bessel function, QRNN is with  $1 \times 2 \times 4 \times 3 = 24$  trainable quantum parameters and  $3 \times 1 + 1 = 4$  trainable classical parameters; QGRU is with  $3 \times 2 \times 4 \times 3 = 72$  trainable quantum parameters and  $3 \times 1 + 1 = 4$  trainable classical parameters; QLSTM is with  $6 \times 2 \times 4 \times 3 = 144$  trainable quantum parameters and  $4 \times 1 + 1 = 5$  trainable classical parameters. For time-series prediction tasks such as NARMA5 and NARMA10, the number of trainable quantum parameters are 48, 144 and 288 for QRNN, QGRU and QLSTM, respectively.

The optimizer used for this experiment is RMSprop [111], a variant of gradient descent methods with an adaptive learning rate. The optimizer is configured with the following hyperparameters: learning rate  $\eta = 0.01$ , smoothing constant  $\alpha = 0.99$ , and  $\epsilon = 10^{-8}$ .

### B. Reservoir Computing

The RC experiments are configured with the same hyperparameters as the full optimization cases in Section V A. The only difference is that all the quantum parameters are frozen after the random initialization. Therefore, only classical parameters are trainable.

### C. Noisy Simulation

We used a noise model consisting of serial thermal relaxation and depolarization noise channels, an approach supported by [112] [113]. We use high-performance noise model parameters that are largely based on the upper limit performance of the IBM Peekskill superconducting quantum device, currently in exploratory mode. For the thermal relaxation

noise channel, T1 and T2 coherence times were sampled per qubit from  $\mathcal{N}(500\mu s, 50\mu s)$  and  $\mathcal{N}(400\mu s, 40\mu s)$ , respectively, where  $\mathcal{N}(\mu, \sigma)$  denotes a normal distribution. Quantum gate and instruction times were fixed values of 0 ns for the  $R_Z$  virtual gate, 20 ns for X90 gate, 300 ns for CNOT gate, 700 ns for measurement and 800 ns for reset instruction. Depolarization channel parameters, single-qubit errors and CNOT gate errors were sampled from  $\mathcal{N}(1 \times 10^{-4}, 1 \times 10^{-5})$  and  $\mathcal{N}(1 \times 10^{-3}, 1 \times 10^{-4})$ , respectively.

#### D. Classical RNN Baseline

We set the classical RNN, GRU and LSTM with the following model size to be the baseline in this study. The model sizes (number of parameters) are set to be similar to their quantum counterpart to investigate the learning capabilities of these models. For the experiments considered in this paper: RNN is with 40 parameters in RNN and 6 parameters in the final linear layer; GRU is with 120 parameters in GRU and 6 parameters in the final linear layer; LSTM is with 160 parameters in LSTM and 6 parameters in the final linear layer. Similar to the setting in quantum models, RC training means the recurrent parameters are frozen after randomly initialized and only final linear layers are trained.

#### E. Tasks

##### 1. Function Approximation-Damped SHM

Damped harmonic oscillators can be used to describe or approximate a wide range of systems, including the mass on a string and acoustic systems. Damped harmonic oscillation can be described by the equation:

$$\frac{d^2x}{dt^2} + 2\zeta\omega_0 \frac{dx}{dt} + \omega_0^2 x = 0, \quad (9)$$

where  $\omega_0 = \sqrt{\frac{k}{m}}$  is the (undamped) system's characteristic frequency and  $\zeta = \frac{c}{2\sqrt{mk}}$  is the damping ratio. In this paper, we consider a specific example from the simple pendulum with the following formulation:

$$\frac{d^2\theta}{dt^2} + \frac{b}{m} \frac{d\theta}{dt} + \frac{g}{L} \sin \theta = 0, \quad (10)$$

in which the gravitational constant  $g = 9.81$ , the damping factor  $b = 0.15$ , the pendulum length  $l = 1$  and mass  $m = 1$ . The initial condition at  $t = 0$  has angular displacement

$\theta = 0$ , and the angular velocity  $\dot{\theta} = 3$  rad/sec. We present the quantum learning result of the angular velocity  $\dot{\theta}$ .

## 2. Function Approximation-Bessel Function

Bessel functions are also commonly encountered in physics and engineering problems, such as electromagnetic fields or heat conduction in a cylindrical geometry. Bessel functions of the first kind,  $J_\alpha(x)$ , are solutions to the Bessel differential equation

$$x^2 \frac{d^2 y}{dx^2} + x \frac{dy}{dx} + (x^2 - \alpha^2) y = 0, \quad (11)$$

and can be defined as

$$J_\alpha(x) = \sum_{m=0}^{\infty} \frac{(-1)^m}{m! \Gamma(m + \alpha + 1)} \left(\frac{x}{2}\right)^{2m + \alpha}, \quad (12)$$

where  $\Gamma(x)$  is the Gamma function.

In this paper, we choose  $J_2$  as the function used for training.

## 3. Time Series Prediction (NARMA Benchmark)

We use NARMA (Non-linear Auto-Regressive Moving Average) time series datasets [114] for this task. The NARMA series that we use in this work can be defined by [115]:

$$y_{t+1} = \alpha y_t + \beta y_t \left( \sum_{j=0}^{n_o-1} y_{t-j} \right) + \gamma u_{t-n_o+1} u_t + \delta \quad (13)$$

where  $(\alpha, \beta, \gamma, \delta) = (0.3, 0.05, 1.5, 0.1)$  and  $n_o$  is used to determine the nonlinearity. The input  $\{u_t\}_{t=1}^M$  for the NARMA tasks is:

$$u_t = 0.1 \left( \sin \left( \frac{2\pi \bar{\alpha} t}{T} \right) \sin \left( \frac{2\pi \bar{\beta} t}{T} \right) \sin \left( \frac{2\pi \bar{\gamma} t}{T} \right) + 1 \right) \quad (14)$$

where  $(\bar{\alpha}, \bar{\beta}, \bar{\gamma}, T) = (2.11, 3.73, 4.11, 100)$  as used in [116]. We set the length of inputs and outputs to  $M = 300$ . In this paper, we consider  $n_o = 5$  and  $n_o = 10$ , NARMA5 and NARMA10 respectively.

## VI. RESULTS

In the results we present here, the orange dashed line represents the ground truth while the blue solid line is the output from the models. The vertical red dashed line separates the *training* set (left) from the *testing* set (right). For all datasets we consider in this paper, 67% are used for the training and the remaining 33% are for testing.

### A. Function Approximation

#### 1. QRNN

For the QRNN, we observe similar results in both the damped SHM (Figure 7) and Bessel function (Figure 8) cases. Both the QRNN-RC and QRNN learn the important features after single training epochs. However, the fully trained QRNN captures more amplitude information in the first epoch. This is not surprising since the fully trained one requires more resources to tune all the quantum parameters, while the RC version does not. We observe that QRNN-RC can achieve performance comparable to fully trained QRNN after 15 epochs of training, except some of the large amplitude regions. After the training, the loss of RC and fully trained converge to a low value. In the case of damped SHM, if we compare the QRNN-RC to classical RNN-RC and RNN, we can observe that the QRNN-RC beats RNN-RC even after 100 epochs of training and reaches comparable performance to fully trained RNN. The results are similar in the case of Bessel function case, we observe that QRNN-RC beat RNN-RC from Epoch 1 to Epoch 100. If we further add quantum device noises to the simulation (defined in Section V C), we can observe that both the fully trained and RC QRNN reach pretty good performance after 100 epochs of training (shown in Figure 9). Particularly, in both the damped SHM and Bessel function cases, we see that QRNN-RC can provide smoother outputs than the fully trained QRNN. We summarize the loss values of noise-free and noisy simulations in Table I and Table IV respectively.

#### 2. QGRU

For the QGRU, we observe similar results for both the damped SHM (Figure 10) and Bessel function (Figure 11) cases. After the first epoch of training, we can observe that the

Dataset	Model	Reservoir	Epoch 1	Epoch 15	Epoch 30	Epoch 100
Damped SHM	QRNN	True	$1.72 \times 10^{-1}/2.21 \times 10^{-2}$	$1.81 \times 10^{-2}/5.17 \times 10^{-3}$	$1.81 \times 10^{-2}/4.96 \times 10^{-3}$	$1.18 \times 10^{-2}/4.91 \times 10^{-3}$
Damped SHM	QRNN	False	$1.01 \times 10^{-1}/5.04 \times 10^{-3}$	$7.19 \times 10^{-3}/9.06 \times 10^{-4}$	$1.87 \times 10^{-3}/2.16 \times 10^{-5}$	$6.8 \times 10^{-4}/4.89 \times 10^{-5}$
Damped SHM	RNN	True	$2.02 \times 10^{-1}/6.46 \times 10^{-2}$	$1.29 \times 10^{-1}/2.68 \times 10^{-2}$	$9.49 \times 10^{-2}/1.97 \times 10^{-2}$	$2.87 \times 10^{-2}/5.87 \times 10^{-3}$
Damped SHM	RNN	False	$7.22 \times 10^{-1}/6.78 \times 10^{-2}$	$1.66 \times 10^{-2}/4.04 \times 10^{-3}$	$2.82 \times 10^{-3}/9.40 \times 10^{-4}$	$1.69 \times 10^{-3}/3.60 \times 10^{-4}$
Bessel	QRNN	True	$1.77 \times 10^{-1}/2.91 \times 10^{-2}$	$1.65 \times 10^{-2}/3.60 \times 10^{-3}$	$1.53 \times 10^{-2}/3.61 \times 10^{-3}$	$1.52 \times 10^{-2}/3.57 \times 10^{-3}$
Bessel	QRNN	False	$4.16 \times 10^{-2}/5.54 \times 10^{-3}$	$5.10 \times 10^{-3}/6.08 \times 10^{-4}$	$1.40 \times 10^{-3}/3.19 \times 10^{-5}$	$6.45 \times 10^{-4}/2.62 \times 10^{-5}$
Bessel	RNN	True	$5.22 \times 10^{-1}/1.65 \times 10^{-1}$	$7.82 \times 10^{-2}/1.93 \times 10^{-2}$	$7.11 \times 10^{-2}/1.76 \times 10^{-2}$	$4.37 \times 10^{-2}/1.11 \times 10^{-2}$
Bessel	RNN	False	$1.79 \times 10^{-1}/2.93 \times 10^{-2}$	$3.80 \times 10^{-3}/2.83 \times 10^{-4}$	$4.49 \times 10^{-3}/3.25 \times 10^{-3}$	$3.05 \times 10^{-4}/1.79 \times 10^{-5}$
NARMA5	QRNN	True	$2.72 \times 10^{-3}/2.93 \times 10^{-4}$	$1.03 \times 10^{-4}/7.28 \times 10^{-5}$	$1.26 \times 10^{-4}/3.44 \times 10^{-5}$	$1.40 \times 10^{-4}/4.13 \times 10^{-5}$
NARMA5	QRNN	False	$3.19 \times 10^{-2}/1.82 \times 10^{-4}$	$3.26 \times 10^{-4}/9.52 \times 10^{-5}$	$1.57 \times 10^{-4}/4.64 \times 10^{-5}$	$1.84 \times 10^{-4}/4.63 \times 10^{-5}$
NARMA5	RNN	True	$2.73 \times 10^{-2}/7.02 \times 10^{-3}$	$1.78 \times 10^{-4}/7.28 \times 10^{-5}$	$1.73 \times 10^{-4}/7.07 \times 10^{-5}$	$1.45 \times 10^{-4}/6.01 \times 10^{-5}$
NARMA5	RNN	False	$1.03 \times 10^{-1}/2.94 \times 10^{-2}$	$3.47 \times 10^{-4}/1.37 \times 10^{-4}$	$3.27 \times 10^{-4}/1.29 \times 10^{-4}$	$2.44 \times 10^{-4}/9.76 \times 10^{-5}$
NARMA10	QRNN	True	$1.00 \times 10^{-1}/8.73 \times 10^{-3}$	$2.22 \times 10^{-4}/7.99 \times 10^{-5}$	$2.63 \times 10^{-4}/9.42 \times 10^{-5}$	$3.03 \times 10^{-4}/1.24 \times 10^{-4}$
NARMA10	QRNN	False	$3.54 \times 10^{-2}/1.03 \times 10^{-4}$	$3.27 \times 10^{-4}/1.96 \times 10^{-4}$	$3.65 \times 10^{-4}/1.55 \times 10^{-4}$	$3.99 \times 10^{-4}/1.56 \times 10^{-4}$
NARMA10	RNN	True	$6.87 \times 10^{-2}/6.73 \times 10^{-4}$	$5.82 \times 10^{-4}/1.75 \times 10^{-4}$	$5.80 \times 10^{-4}/1.74 \times 10^{-4}$	$5.70 \times 10^{-4}/1.71 \times 10^{-4}$
NARMA10	RNN	False	$2.70 \times 10^{-1}/5.75 \times 10^{-2}$	$5.25 \times 10^{-4}/1.57 \times 10^{-4}$	$5.07 \times 10^{-4}/1.51 \times 10^{-4}$	$4.23 \times 10^{-4}/1.27 \times 10^{-4}$

TABLE I. RNN model results for training Epochs 1, 15, 30 and 100.

fully trained QGRU learns more amplitude information than the QGRU-RC, in which only the final linear layer is trained. In the case of damped SHM, we observe that the QGRU-RC can reach comparable performance to QGRU after 15 epochs of training. If we compare the QGRU-RC to classical GRU-RC and GRU, we can observe that the QGRU-RC beats GRU-RC up to the first 30 epochs of training and reaches similar performance to GRU-RC and fully trained GRU after 100 epochs of training. In the case of Bessel function, we observe that QGRU-RC saturates after 15 epochs of training and can capture most of the data, except some of the large amplitude regions. We also observe that the QGRU-RC performs similar to the classical GRU-RC after 15 epochs of training.

If we add quantum device noise to the simulation (defined in Section V C), we observe that both the full optimization and RC training of QGRU under the effect of simulated quantum noises can still reach reasonable performance in both the damped SHM and the Bessel function (shown in Figure 12). Most importantly, we observe that in both the damped SHM and Bessel function cases, the QGRU-RC can generate smoother outputs than the fully optimized QGRU. We summarize the loss values of noise-free and noisy simulations in Table II and Table IV respectively.

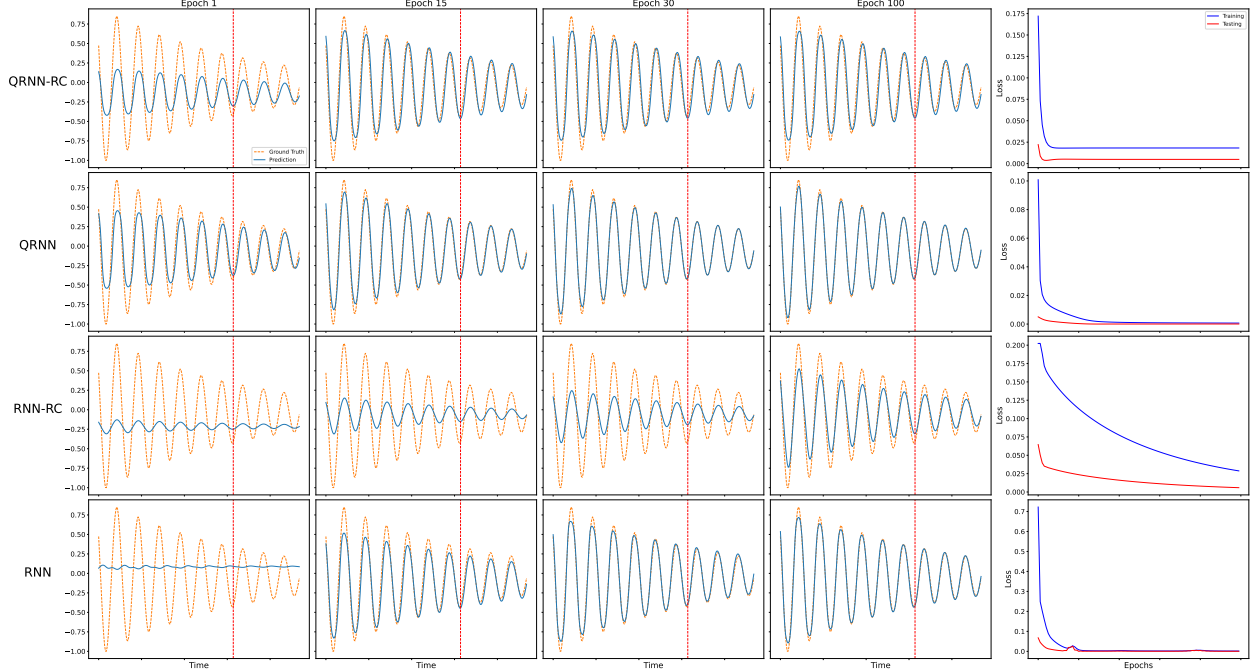


FIG. 7. Learning the damped SHM with QRNN-RC.

### 3. QLSTM

For the QLSTM, we observe similar results in both the damped SHM (Figure 13) and Bessel function (Figure 14) cases. For the damped SHM case, we observe that after the first epoch of training, the fully trained QLSTM learns more amplitude information than the QLSTM-RC in which only the final linear layer is trained. While in the Bessel function case, the QLSTM-RC and QLSTM provide similar learning outcomes in the first training epoch. We observe that both models reach similar results after 100 epochs of training. However, the loss values of QLSTM are much lower after the training. This is not surprising since all the model parameters are trained in QLSTM while in QLSTM-RC only the final linear layer is trained. If we compare QLSTM-RC to LSTM-RC, we can observe that the quantum version captures more features after the same number of training epochs in both the damped SHM and Bessel function cases. If we add quantum device noise to the simulation (defined in Section V C), we observe that the both the full optimization and RC training of QLSTM under the effect of simulated quantum noise can still reach reasonable performance in both the damped SHM and the Bessel function (shown in Figure 15). We observe that in both the damped SHM and Bessel function cases, the QLSTM-RC can generate

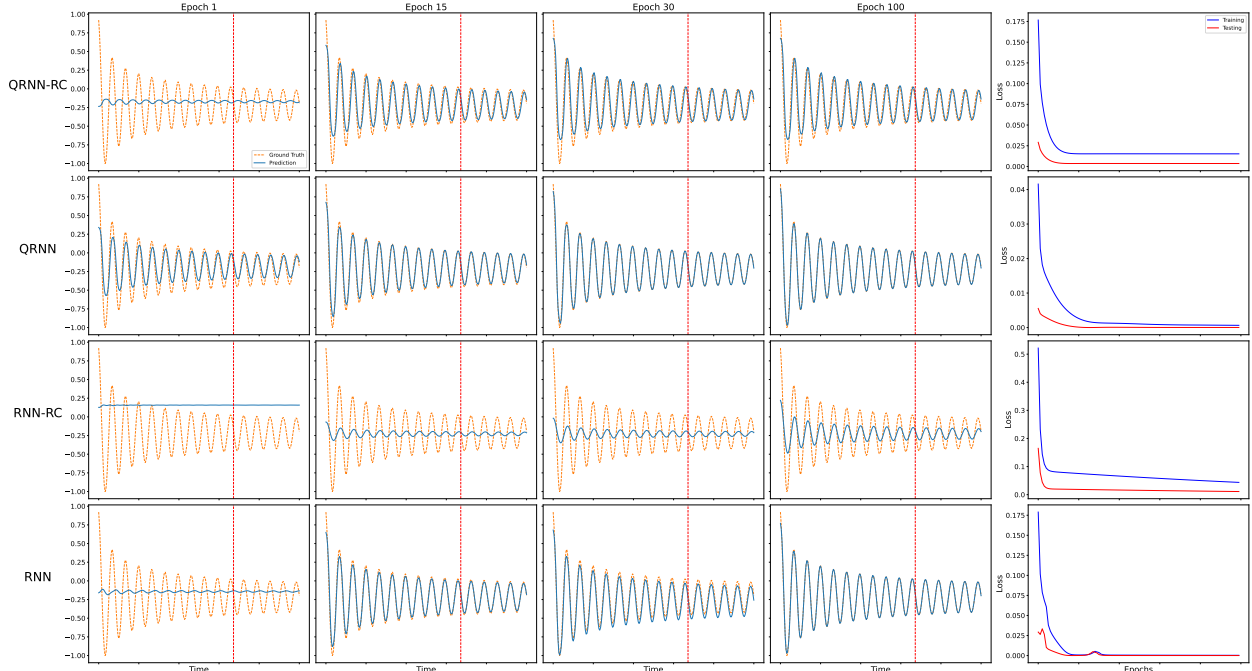


FIG. 8. Learning the Bessel function with QRNN-RC.

smoother outputs than the fully optimized QLSTM. The results are consistent with QRNN and QGRU. We summarize the loss values of noise-free and noisy simulations in Table III and Table IV respectively.

## B. Time-Series Prediction-NARMA benchmark

We further investigate the time-series prediction task with NARMA benchmarks (described in Section V E 3).

### 1. QRNN

For QRNN, we observe that in both the NARMA5 and NARMA10 cases (shown in Figure 16 and Figure 17), the QRNN learns more structure of the data in the first training epoch. However, we can see that the QRNN-RC can catch up pretty quickly. After 15 epochs of training, the results from QRNN-RC are very close to QRNN. If we compare the performance of QRNN-RC to classical RNN-RC and RNN, we can see that QRNN-RC provides results superior than classical models with a similar number of parameters.

Dataset	Model	Reservoir	Epoch 1	Epoch 15	Epoch 30	Epoch 100
Damped SHM	QGRU	True	$2.26 \times 10^{-1}/2.78 \times 10^{-2}$	$4.54 \times 10^{-2}/1.31 \times 10^{-2}$	$4.55 \times 10^{-2}/1.30 \times 10^{-2}$	$4.55 \times 10^{-2}/1.29 \times 10^{-2}$
Damped SHM	QGRU	False	$1.97 \times 10^{-1}/1.51 \times 10^{-2}$	$2.01 \times 10^{-2}/3.64 \times 10^{-3}$	$1.04 \times 10^{-2}/1.30 \times 10^{-3}$	$1.39 \times 10^{-3}/1.19 \times 10^{-4}$
Damped SHM	GRU	True	$4.62 \times 10^{-1}/1.18 \times 10^{-1}$	$1.13 \times 10^{-1}/2.26 \times 10^{-2}$	$7.45 \times 10^{-2}/1.50 \times 10^{-2}$	$4.61 \times 10^{-2}/9.92 \times 10^{-3}$
Damped SHM	GRU	False	$2.12 \times 10^{-1}/8.54 \times 10^{-2}$	$2.22 \times 10^{-2}/3.90 \times 10^{-3}$	$2.94 \times 10^{-3}/1.80 \times 10^{-4}$	$4.51 \times 10^{-4}/7.75 \times 10^{-5}$
Bessel	QGRU	True	$1.54 \times 10^{-1}/2.58 \times 10^{-2}$	$3.90 \times 10^{-2}/9.92 \times 10^{-3}$	$3.82 \times 10^{-2}/9.90 \times 10^{-3}$	$3.82 \times 10^{-2}/9.89 \times 10^{-3}$
Bessel	QGRU	False	$5.53 \times 10^{-2}/9.39 \times 10^{-3}$	$1.10 \times 10^{-2}/2.05 \times 10^{-3}$	$2.94 \times 10^{-3}/9.69 \times 10^{-5}$	$1.31 \times 10^{-3}/1.37 \times 10^{-5}$
Bessel	GRU	True	$1.71 \times 10^{-1}/3.33 \times 10^{-2}$	$4.16 \times 10^{-2}/1.13 \times 10^{-2}$	$3.78 \times 10^{-2}/1.05 \times 10^{-2}$	$3.05 \times 10^{-2}/8.51 \times 10^{-3}$
Bessel	GRU	False	$1.03 \times 10^{-1}/9.98 \times 10^{-2}$	$1.98 \times 10^{-2}/4.77 \times 10^{-3}$	$4.62 \times 10^{-3}/1.72 \times 10^{-3}$	$4.68 \times 10^{-4}/9.09 \times 10^{-6}$
NARMA5	QGRU	True	$9.48 \times 10^{-2}/6.59 \times 10^{-3}$	$6.46 \times 10^{-5}/3.21 \times 10^{-5}$	$8.62 \times 10^{-5}/2.36 \times 10^{-5}$	$1.10 \times 10^{-4}/3.50 \times 10^{-5}$
NARMA5	QGRU	False	$4.12 \times 10^{-3}/5.58 \times 10^{-5}$	$1.53 \times 10^{-4}/3.22 \times 10^{-5}$	$1.36 \times 10^{-4}/2.41 \times 10^{-5}$	$1.22 \times 10^{-4}/3.55 \times 10^{-5}$
NARMA5	GRU	True	$1.90 \times 10^{-3}/2.23 \times 10^{-2}$	$3.62 \times 10^{-4}/1.45 \times 10^{-4}$	$3.46 \times 10^{-4}/1.39 \times 10^{-4}$	$2.69 \times 10^{-4}/1.09 \times 10^{-4}$
NARMA5	GRU	False	$9.00 \times 10^{-2}/6.43 \times 10^{-4}$	$2.63 \times 10^{-4}/1.04 \times 10^{-4}$	$2.36 \times 10^{-4}/9.39 \times 10^{-5}$	$1.22 \times 10^{-4}/4.99 \times 10^{-5}$
NARMA10	QGRU	True	$1.54 \times 10^{-3}/2.91 \times 10^{-4}$	$2.20 \times 10^{-4}/7.22 \times 10^{-5}$	$2.50 \times 10^{-4}/9.23 \times 10^{-5}$	$2.74 \times 10^{-4}/1.21 \times 10^{-4}$
NARMA10	QGRU	False	$6.30 \times 10^{-3}/1.28 \times 10^{-4}$	$3.63 \times 10^{-4}/1.14 \times 10^{-4}$	$4.04 \times 10^{-4}/1.20 \times 10^{-4}$	$2.97 \times 10^{-4}/1.25 \times 10^{-4}$
NARMA10	GRU	True	$2.08 \times 10^{-1}/8.04 \times 10^{-2}$	$2.25 \times 10^{-4}/8.21 \times 10^{-5}$	$2.18 \times 10^{-4}/7.57 \times 10^{-5}$	$2.14 \times 10^{-4}/7.50 \times 10^{-5}$
NARMA10	GRU	False	$5.39 \times 10^{-1}/6.93 \times 10^{-2}$	$2.56 \times 10^{-4}/8.03 \times 10^{-5}$	$2.52 \times 10^{-4}/7.94 \times 10^{-5}$	$2.32 \times 10^{-4}/7.47 \times 10^{-5}$

TABLE II. GRU model results for training Epochs 1, 15, 30 and 100.

Dataset	Model	Reservoir	Epoch 1	Epoch 15	Epoch 30	Epoch 100
Damped SHM	QLSTM	True	$3.19 \times 10^{-1}/5.86 \times 10^{-2}$	$6.42 \times 10^{-2}/1.08 \times 10^{-2}$	$5.55 \times 10^{-2}/1.38 \times 10^{-2}$	$5.55 \times 10^{-2}/1.41 \times 10^{-2}$
Damped SHM	QLSTM	False	$1.66 \times 10^{-1}/1.35 \times 10^{-2}$	$2.89 \times 10^{-2}/5.53 \times 10^{-3}$	$9.06 \times 10^{-3}/3.41 \times 10^{-4}$	$2.86 \times 10^{-3}/1.94 \times 10^{-4}$
Damped SHM	LSTM	True	$3.45 \times 10^{-1}/7.49 \times 10^{-2}$	$1.89 \times 10^{-1}/3.98 \times 10^{-2}$	$1.66 \times 10^{-1}/3.51 \times 10^{-2}$	$1.10 \times 10^{-1}/2.32 \times 10^{-2}$
Damped SHM	LSTM	False	$3.32 \times 10^{-1}/3.29 \times 10^{-2}$	$3.65 \times 10^{-2}/7.38 \times 10^{-3}$	$6.74 \times 10^{-3}/7.27 \times 10^{-4}$	$2.32 \times 10^{-3}/1.68 \times 10^{-3}$
Bessel	QLSTM	True	$7.53 \times 10^{-2}/1.36 \times 10^{-2}$	$3.94 \times 10^{-2}/9.67 \times 10^{-3}$	$3.90 \times 10^{-2}/1.01 \times 10^{-2}$	$3.90 \times 10^{-2}/1.02 \times 10^{-2}$
Bessel	QLSTM	False	$1.04 \times 10^{-1}/1.66 \times 10^{-2}$	$2.30 \times 10^{-2}/5.35 \times 10^{-3}$	$1.27 \times 10^{-2}/2.42 \times 10^{-3}$	$6.97 \times 10^{-4}/1.21 \times 10^{-5}$
Bessel	LSTM	True	$1.21 \times 10^{-1}/2.46 \times 10^{-2}$	$6.58 \times 10^{-2}/1.65 \times 10^{-2}$	$5.43 \times 10^{-2}/1.39 \times 10^{-2}$	$3.76 \times 10^{-2}/1.02 \times 10^{-2}$
Bessel	LSTM	False	$3.03 \times 10^{-1}/4.55 \times 10^{-2}$	$3.48 \times 10^{-2}/8.71 \times 10^{-3}$	$6.97 \times 10^{-3}/1.41 \times 10^{-3}$	$1.31 \times 10^{-3}/3.53 \times 10^{-4}$
NARMA5	QLSTM	True	$8.54 \times 10^{-4}/5.40 \times 10^{-4}$	$1.32 \times 10^{-4}/1.10 \times 10^{-4}$	$9.06 \times 10^{-5}/2.96 \times 10^{-5}$	$1.13 \times 10^{-4}/2.58 \times 10^{-5}$
NARMA5	QLSTM	False	$3.99 \times 10^{-3}/4.07 \times 10^{-4}$	$3.30 \times 10^{-4}/4.23 \times 10^{-4}$	$1.86 \times 10^{-4}/2.06 \times 10^{-4}$	$9.85 \times 10^{-5}/2.52 \times 10^{-5}$
NARMA5	LSTM	True	$4.15 \times 10^{-2}/2.10 \times 10^{-4}$	$3.73 \times 10^{-4}/1.48 \times 10^{-4}$	$3.72 \times 10^{-4}/1.48 \times 10^{-4}$	$3.65 \times 10^{-4}/1.45 \times 10^{-4}$
NARMA5	LSTM	False	$1.19 \times 10^{-1}/7.97 \times 10^{-4}$	$3.34 \times 10^{-4}/1.38 \times 10^{-4}$	$2.93 \times 10^{-4}/1.15 \times 10^{-4}$	$1.91 \times 10^{-4}/8.78 \times 10^{-5}$
NARMA10	QLSTM	True	$1.97 \times 10^{-3}/2.78 \times 10^{-4}$	$3.01 \times 10^{-4}/1.39 \times 10^{-4}$	$2.36 \times 10^{-4}/8.78 \times 10^{-5}$	$2.59 \times 10^{-4}/9.64 \times 10^{-5}$
NARMA10	QLSTM	False	$4.19 \times 10^{-3}/4.71 \times 10^{-4}$	$3.35 \times 10^{-4}/4.73 \times 10^{-4}$	$3.20 \times 10^{-4}/3.74 \times 10^{-4}$	$2.59 \times 10^{-4}/9.50 \times 10^{-5}$
NARMA10	LSTM	True	$1.16 \times 10^{-2}/4.50 \times 10^{-3}$	$4.26 \times 10^{-4}/1.27 \times 10^{-4}$	$4.17 \times 10^{-4}/1.25 \times 10^{-4}$	$3.74 \times 10^{-4}/1.12 \times 10^{-4}$
NARMA10	LSTM	False	$1.70 \times 10^{-1}/4.21 \times 10^{-4}$	$2.94 \times 10^{-4}/8.68 \times 10^{-5}$	$2.76 \times 10^{-4}/8.53 \times 10^{-5}$	$2.31 \times 10^{-4}/8.12 \times 10^{-5}$

TABLE III. LSTM model results for training Epochs 1, 15, 30 and 100.

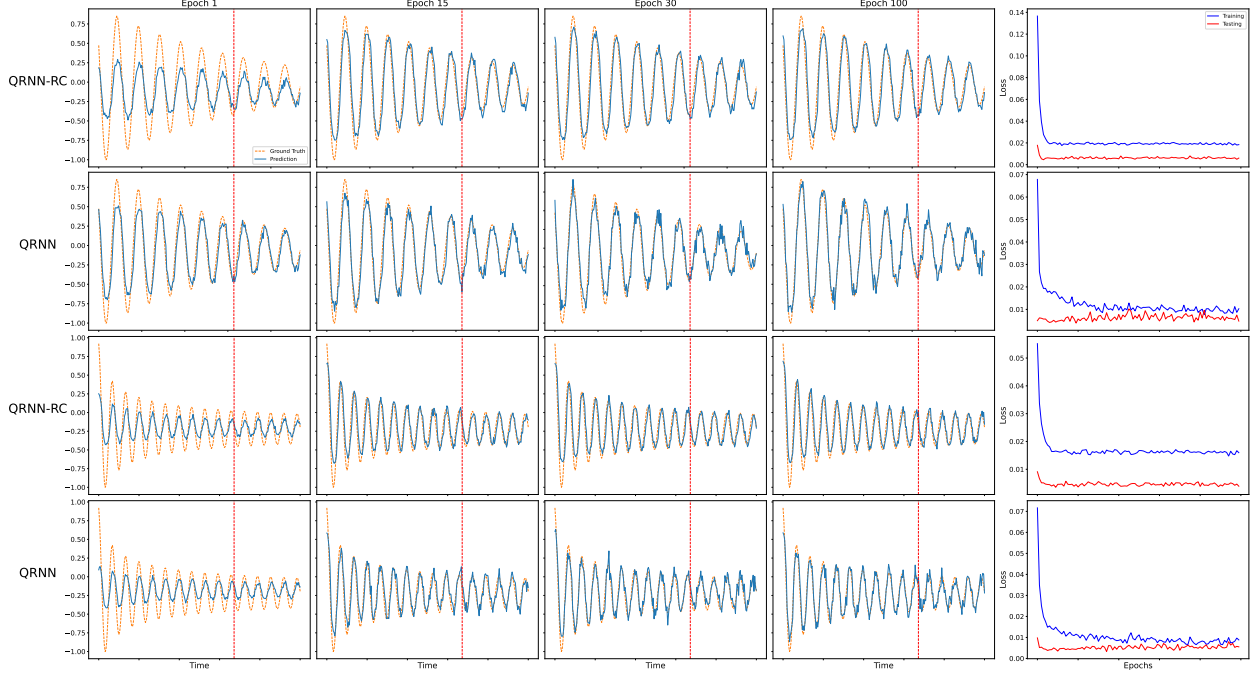


FIG. 9. Noisy simulation of QRNN.

Data	Model	Reservoir	Epoch 1	Epoch 15	Epoch 30	Epoch 100
Bessel	GRU	False	$3.88 \times 10^{-2}/9.71 \times 10^{-3}$	$1.33 \times 10^{-2}/4.7 \times 10^{-3}$	$9.65 \times 10^{-3}/5.32 \times 10^{-3}$	$5.43 \times 10^{-3}/4.47 \times 10^{-3}$
Bessel	GRU	True	$5.18 \times 10^{-2}/1.3 \times 10^{-2}$	$3.72 \times 10^{-2}/1.05 \times 10^{-2}$	$3.74 \times 10^{-2}/1.05 \times 10^{-2}$	$3.67 \times 10^{-2}/1.0 \times 10^{-2}$
Bessel	LSTM	False	$7.77 \times 10^{-2}/1.96 \times 10^{-2}$	$2.74 \times 10^{-2}/9.08 \times 10^{-3}$	$2.5 \times 10^{-2}/1.21 \times 10^{-2}$	$1.49 \times 10^{-2}/7.69 \times 10^{-3}$
Bessel	LSTM	True	$6.16 \times 10^{-2}/1.4 \times 10^{-2}$	$4.02 \times 10^{-2}/1.55 \times 10^{-2}$	$3.89 \times 10^{-2}/1.58 \times 10^{-2}$	$4.18 \times 10^{-2}/1.28 \times 10^{-2}$
Bessel	RNN	False	$4.27 \times 10^{-2}/1.0 \times 10^{-2}$	$1.24 \times 10^{-2}/4.43 \times 10^{-3}$	$7.49 \times 10^{-3}/5.23 \times 10^{-3}$	$6.49 \times 10^{-3}/4.95 \times 10^{-3}$
Bessel	RNN	True	$3.77 \times 10^{-2}/8.71 \times 10^{-3}$	$1.69 \times 10^{-2}/4.15 \times 10^{-3}$	$1.61 \times 10^{-2}/4.32 \times 10^{-3}$	$1.62 \times 10^{-2}/4.95 \times 10^{-3}$
Damped SHM	GRU	False	$1.27 \times 10^{-1}/2.47 \times 10^{-2}$	$1.88 \times 10^{-2}/4.18 \times 10^{-3}$	$7.89 \times 10^{-3}/3.32 \times 10^{-3}$	$7.17 \times 10^{-3}/6.49 \times 10^{-3}$
Damped SHM	GRU	True	$8.34 \times 10^{-2}/1.29 \times 10^{-2}$	$4.52 \times 10^{-2}/1.51 \times 10^{-2}$	$4.42 \times 10^{-2}/1.45 \times 10^{-2}$	$4.51 \times 10^{-2}/1.2 \times 10^{-2}$
Damped SHM	LSTM	False	$1.21 \times 10^{-1}/2.19 \times 10^{-2}$	$2.96 \times 10^{-2}/9.09 \times 10^{-3}$	$2.28 \times 10^{-2}/8.77 \times 10^{-3}$	$1.86 \times 10^{-2}/1.41 \times 10^{-2}$
Damped SHM	LSTM	True	$1.18 \times 10^{-1}/2.37 \times 10^{-2}$	$5.92 \times 10^{-2}/1.9 \times 10^{-2}$	$5.96 \times 10^{-2}/1.72 \times 10^{-2}$	$6.01 \times 10^{-2}/1.75 \times 10^{-2}$
Damped SHM	RNN	False	$2.45 \times 10^{-2}/5.18 \times 10^{-3}$	$1.38 \times 10^{-2}/5.48 \times 10^{-3}$	$1.17 \times 10^{-2}/6.43 \times 10^{-3}$	$8.56 \times 10^{-3}/4.95 \times 10^{-3}$
Damped SHM	RNN	True	$7.24 \times 10^{-2}/1.72 \times 10^{-2}$	$1.91 \times 10^{-2}/6.21 \times 10^{-3}$	$1.76 \times 10^{-2}/6.8 \times 10^{-3}$	$1.94 \times 10^{-2}/5.47 \times 10^{-3}$

TABLE IV. Summary of Simulation Results with Quantum Noise Model

## 2. QGRU

For the QGRU, we observe that in both the NARMA5 and NARMA10 cases (shown in Figure 18 and Figure 19), the QGRU learns more structure of the data in the first training epoch. However, we can see that the QGRU-RC can catch up pretty quickly. After 15 epochs of training, the results from QGRU-RC are very similar to the ones from QGRU.

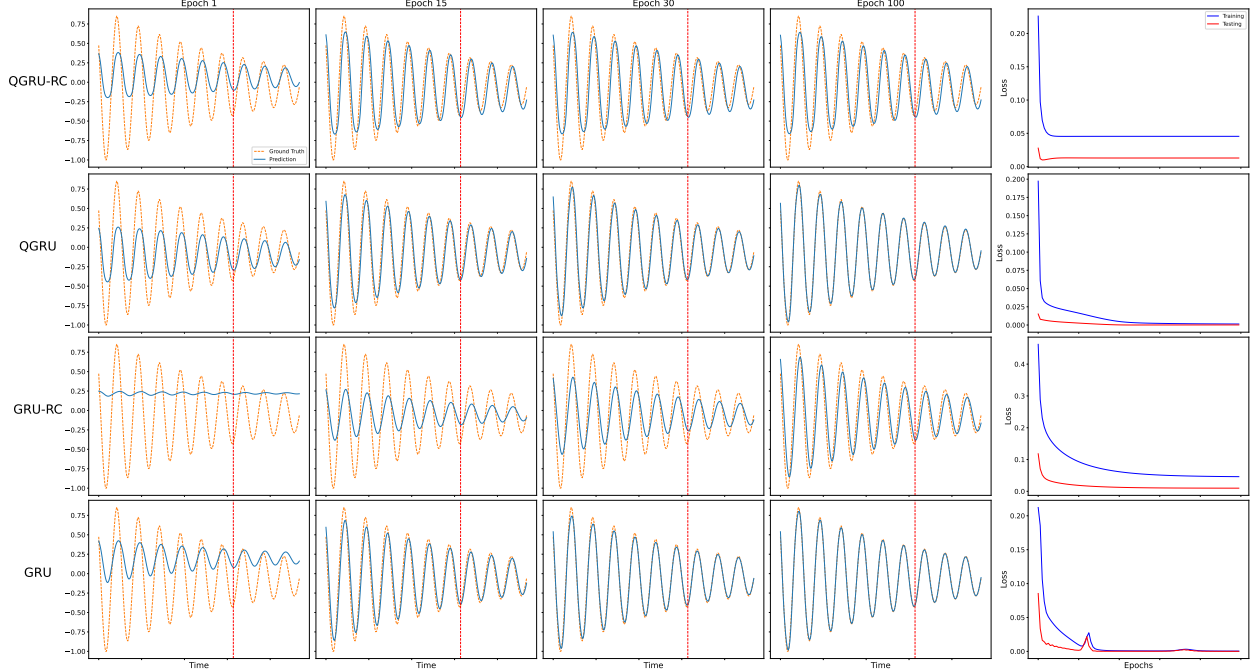


FIG. 10. Learning the damped SHM with QGRU-RC.

We also see that they are indistinguishable after 100 epochs of training. In addition, the simulation shows that the performance of QGRU-RC is superior than the classical GRU-RC and GRU with a similar number of parameters.

### 3. QLSTM

For the QLSTM, we observe that in both the NARMA5 and NARMA10 cases (shown in Figure 20 and Figure 21), the RC and full optimization of QLSTM can reach good performance after 100 epochs of training. Surprisingly, the training performance of QLSTM-RC is better than the fully optimized one as we can see that the QLSTM-RC predicts the sequence better than QLSTM after 30 epochs of training. In addition, we observe that the quantum LSTM, either RC or fully optimized one, perform better than their classical counterparts.

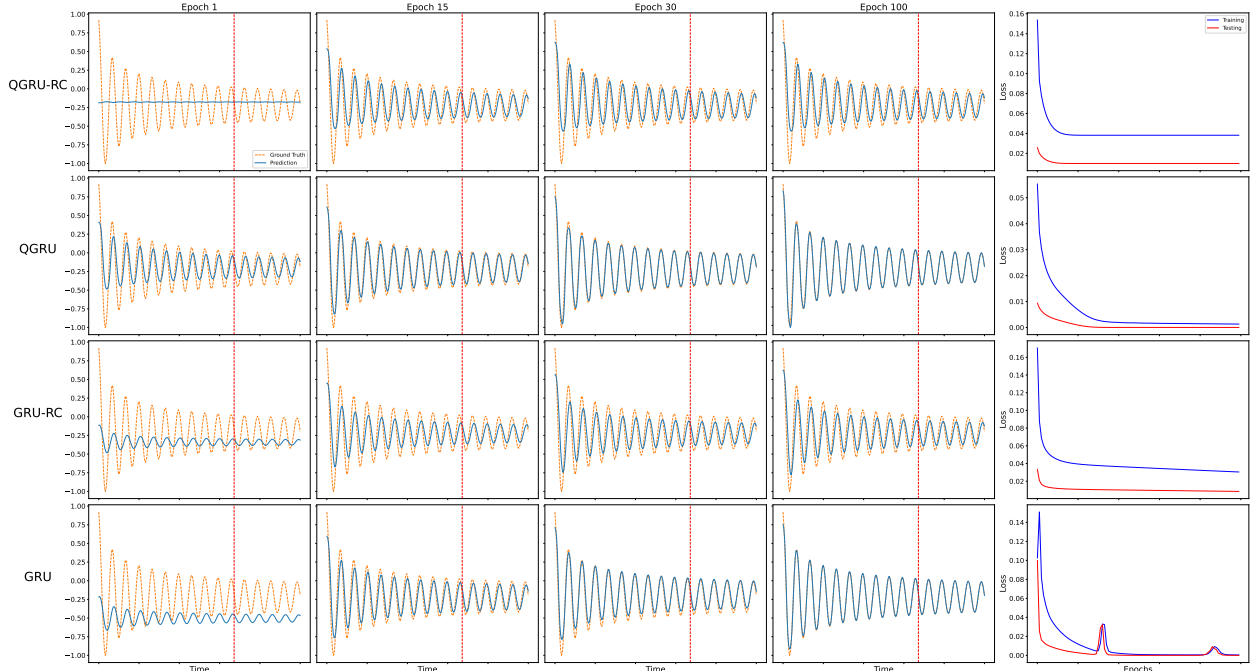


FIG. 11. Learning the Bessel function with QGRU-RC.

## VII. DISCUSSION

### A. Quantum Hardware Efficiency

Quantum hardware efficiency is a quantum algorithm design consideration in which the demands on quantum computing resources are minimized. This is particularly important in the current noisy intermediate-scale quantum (NISQ) era of quantum computing [117]. In this paper we consider that hardware efficiency is achieved by running fewer quantum circuits.

The RC framework demonstrated in this work is well-suited for NISQ computers because hardware efficiency is improved significantly over the original three QRNNs. The clear reason for this improvement is that efficient training is limited to the final layer, meaning that a quantum computer would only be used for generating the outputs for the classical linear layer and the quantum parameters are not trained.

As the RC approach is a hardware efficient approach it reduces the negative effects of noise on the quantum computation and therefore can improve the performance of time-series prediction. In our work, the noisy simulation results in Figures 9, 12, and 15 show that the RC approach, when compared with the original QRNN algorithm, has smoother

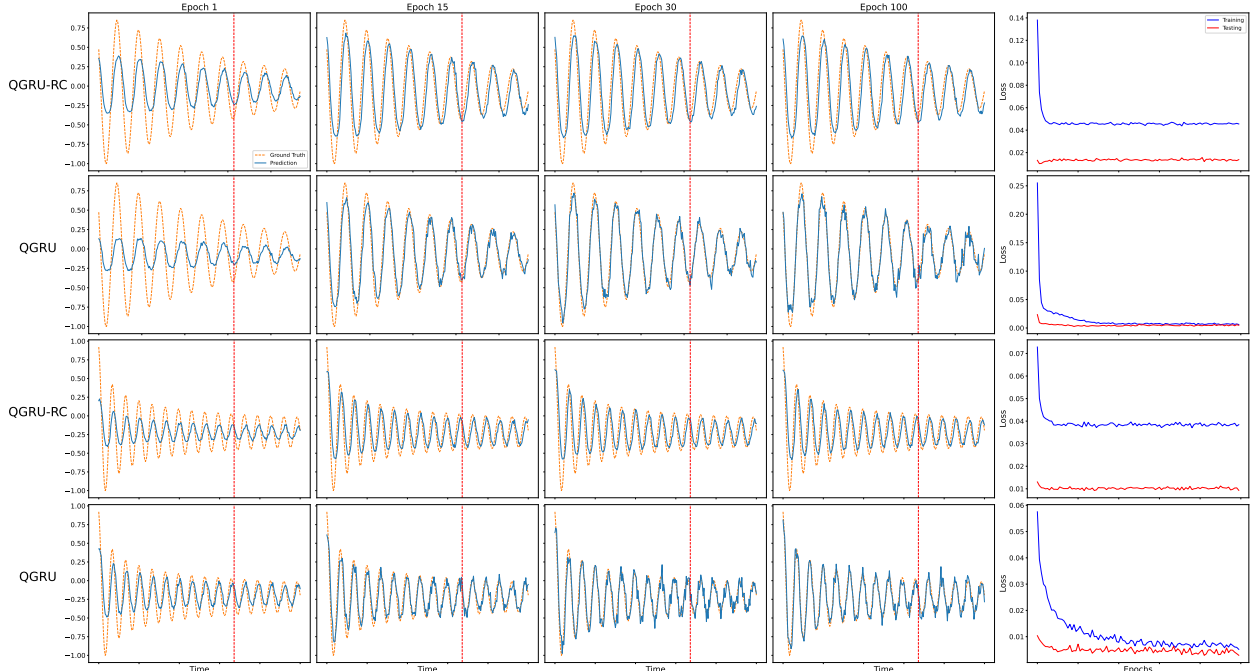


FIG. 12. Noisy simulation of QGRU.

prediction curves that are less corrupted by simulation noise. This is highly desirable given that the target function is smooth. In addition there is evidence that the MSE loss curves, particularly for QRNN-RC in Figure 9, has less noise and stabilizes to a loss minimum in fewer epochs.

## B. Potential Applications

In order to facilitate maximal advantage of a quantum approach to machine learning, the method proposed in this paper can be utilized to decrease the time and complexity required by existing methods for certain applications. In this paper, we analyzed examples of function approximation and time series prediction tasks. This method can further be applied to nuanced tasks using sequential or temporal data, such as using acoustic models for time series classification as implemented in [118], facial recognition systems [61], and natural language processing [98]. Additionally, there are numerous financial applications [119] including time series prediction [42, 43] for stock price and market behavior, and classification problems for risk and fraud detection.

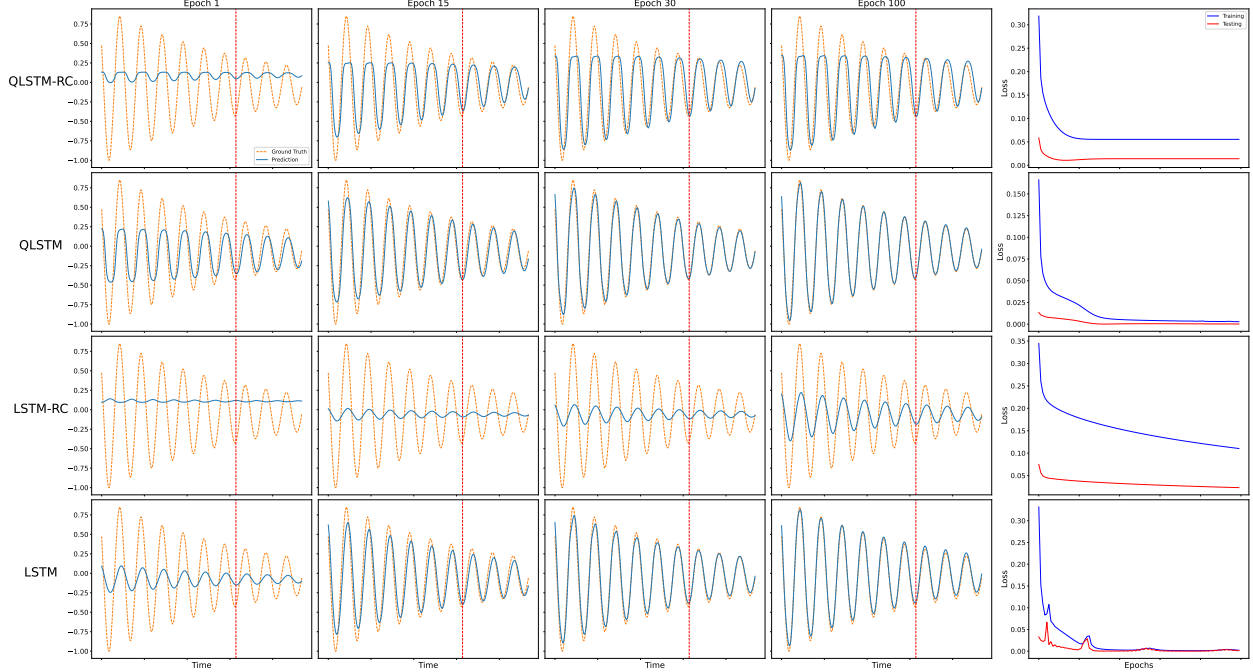


FIG. 13. Learning the damped SHM with QLSTM-RC.

## VIII. CONCLUSION

In this paper, we introduce the function approximation and time-series prediction framework in which the quantum RNN and its variants, such as quantum GRU and quantum LSTM, are used as the reservoir. We show via numerical simulations that the QRNN-RC can reach results comparable to fully trained QRNN models in several function approximation and time-series prediction tasks. Since the QRNNs in the proposed model do not need to be trained, the overall process is much faster than the fully trained ones. We also compare to classical RNN-based RC and show that the quantum solutions require fewer training epochs in most cases. Our results demonstrate a new possibility to utilize quantum neural networks for sequential modeling with very small amount of resource requirement.

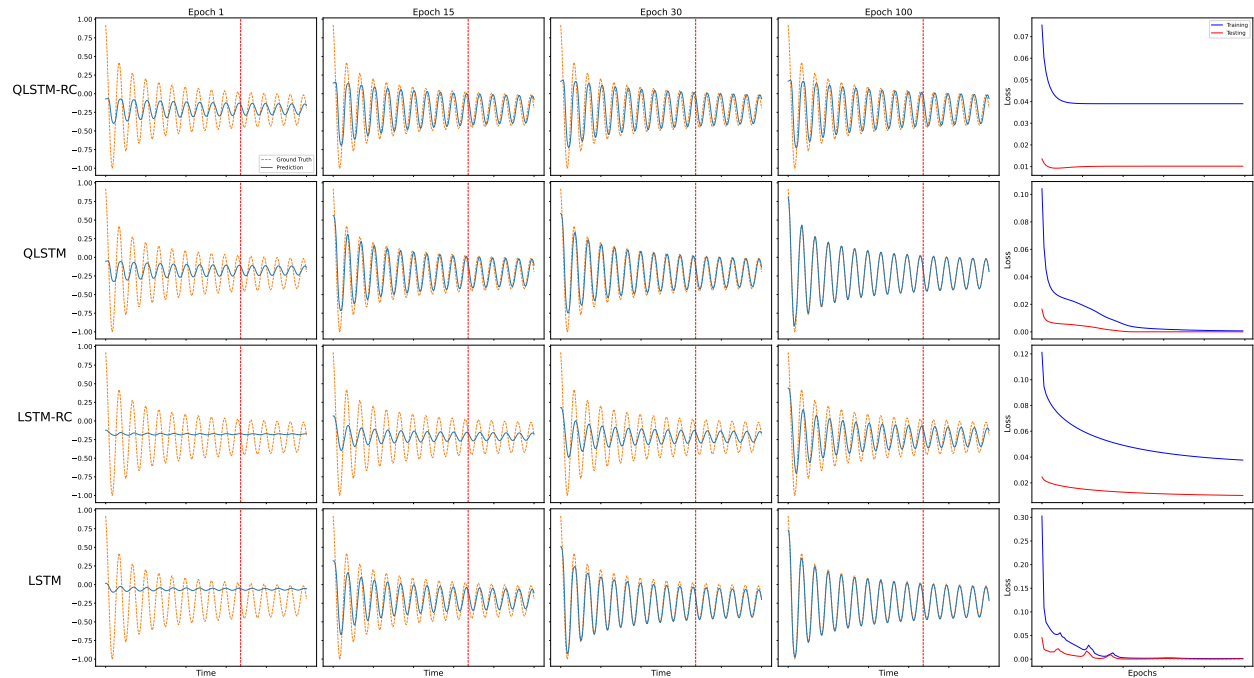


FIG. 14. Learning the Bessel function with QLSTM-RC.

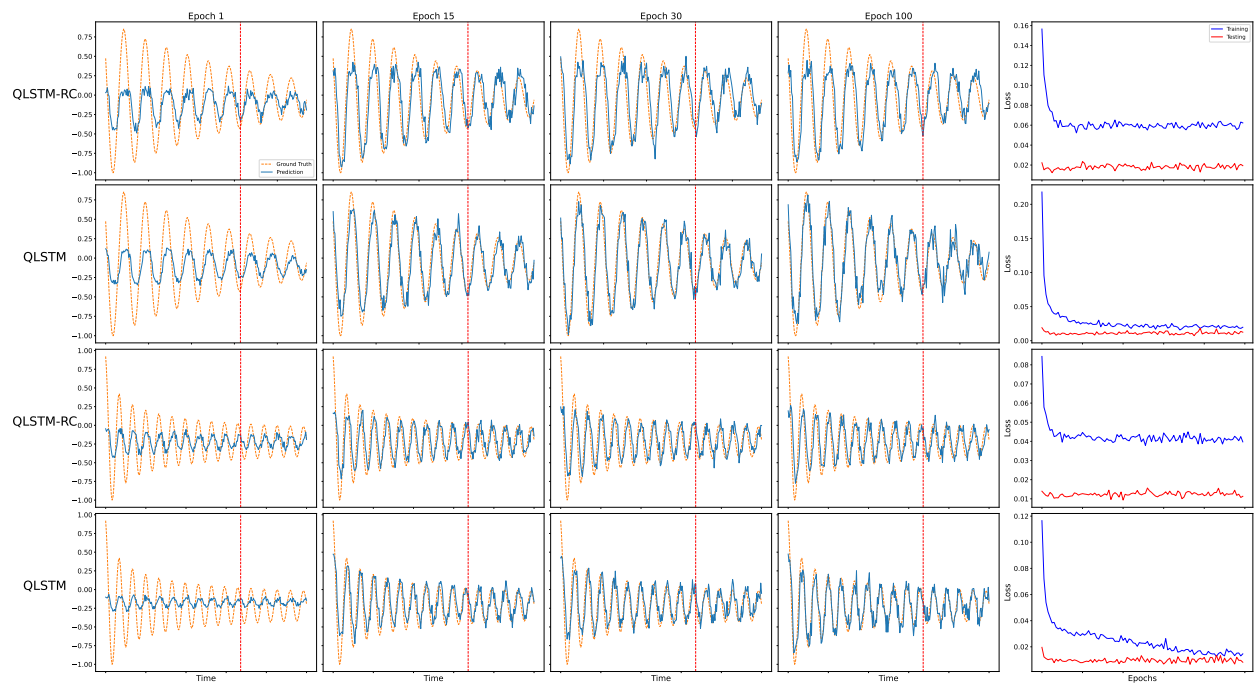


FIG. 15. Noisy simulation of QLSTM.

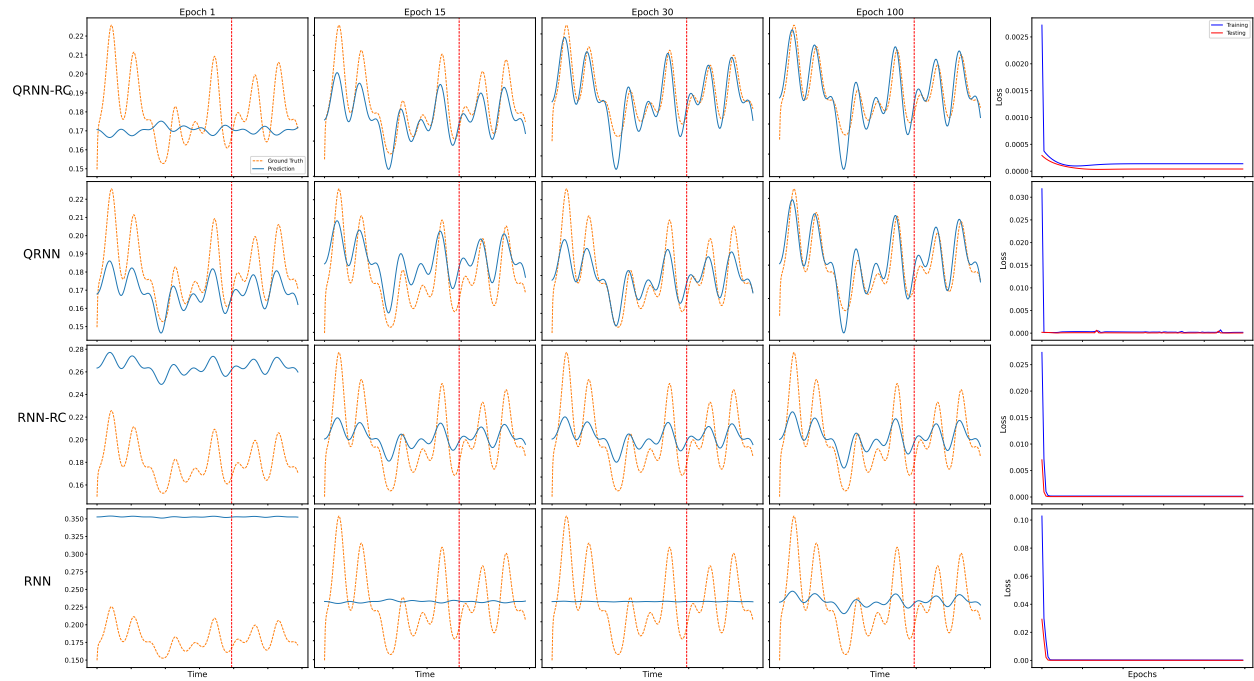


FIG. 16. Learning the NARMA5 with QRNN-RC.

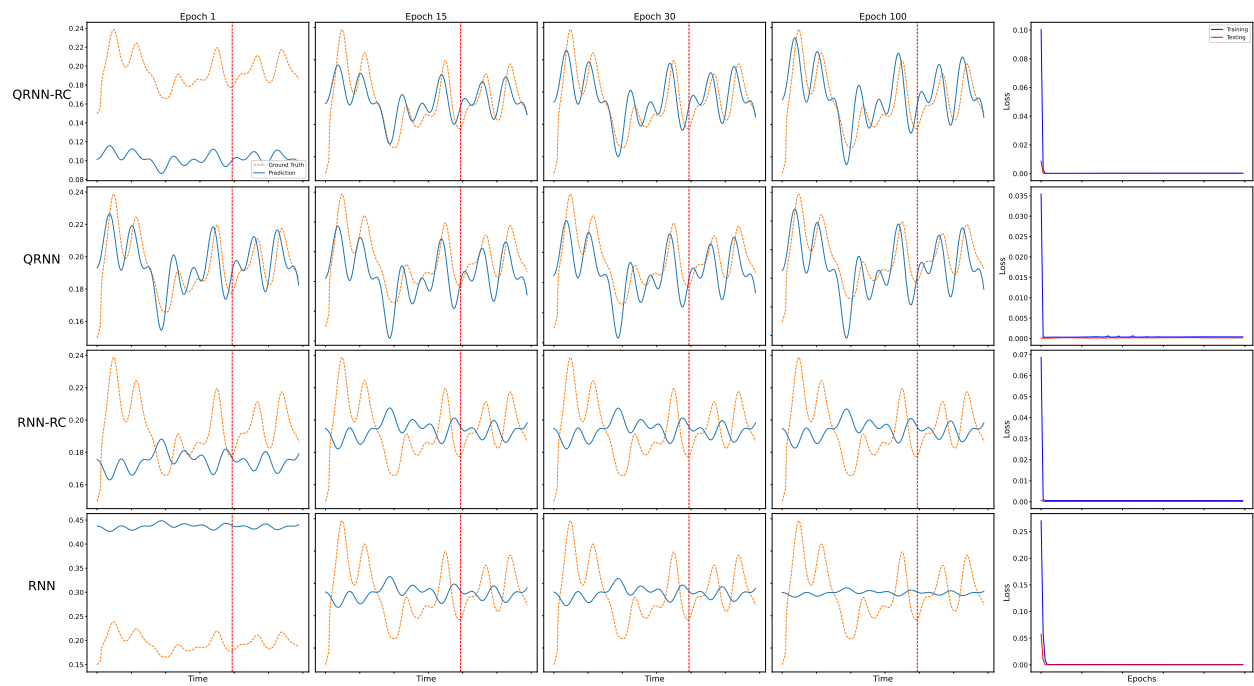
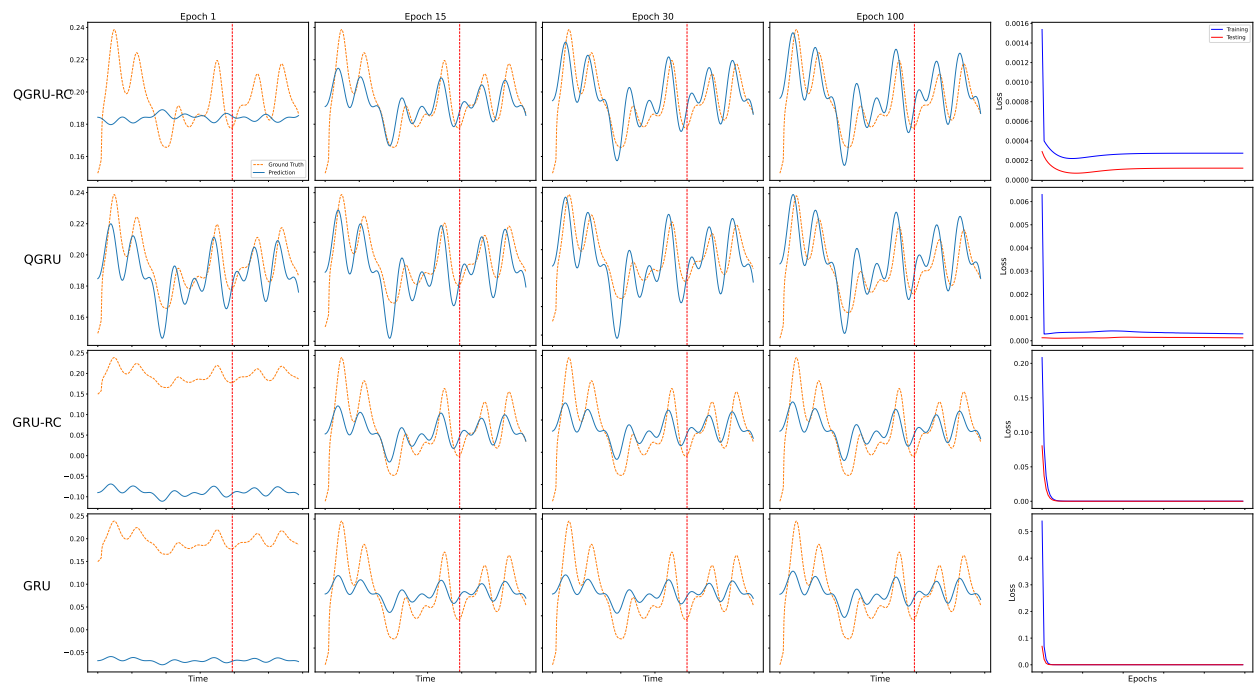
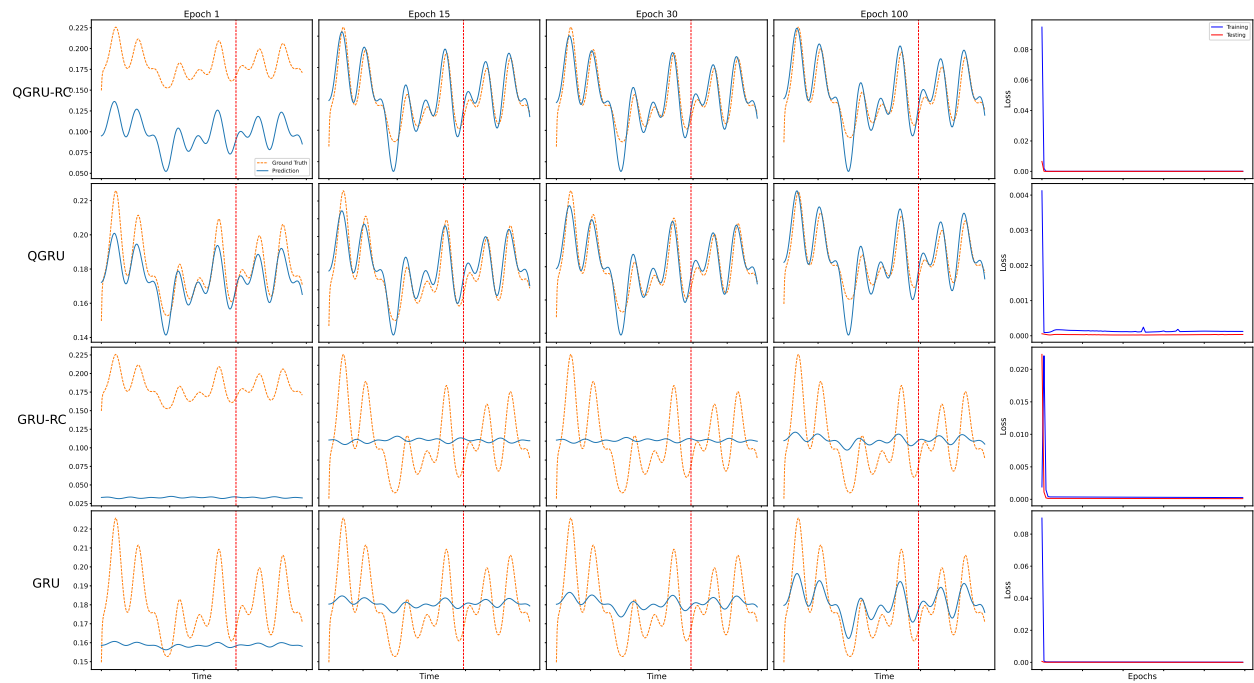


FIG. 17. Learning the NARMA10 with QRNN-RC.



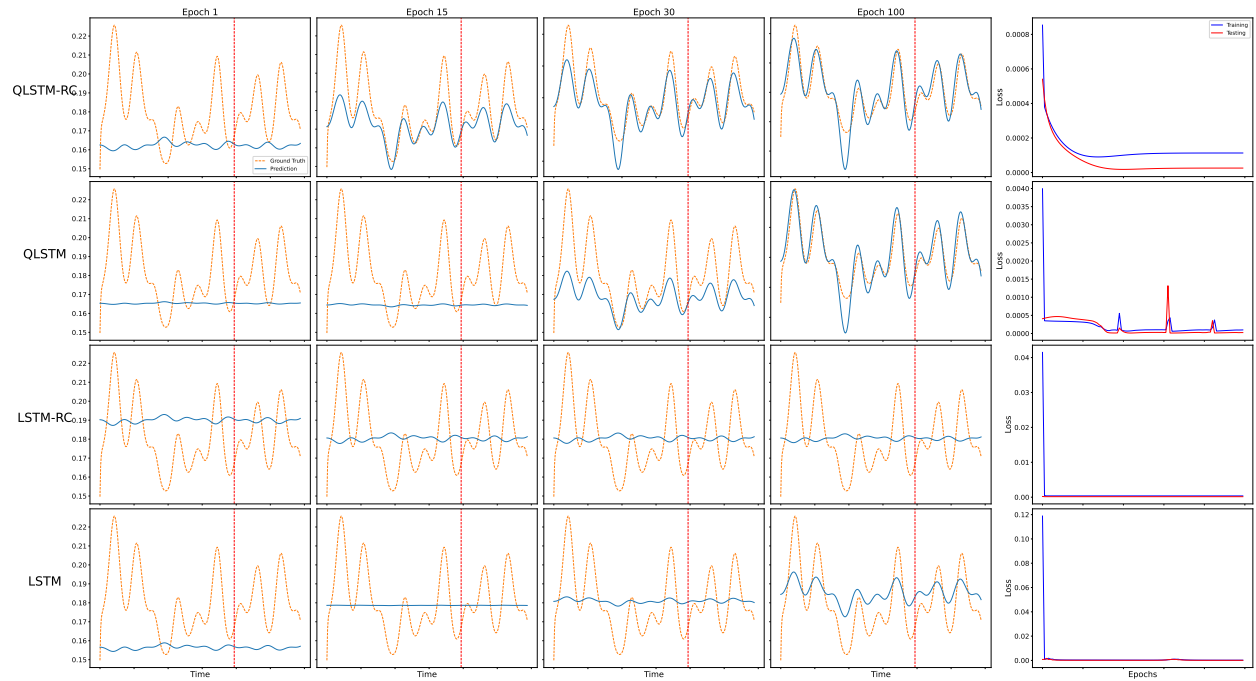


FIG. 20. Learning the NARMA5 with QLSTM-RC.

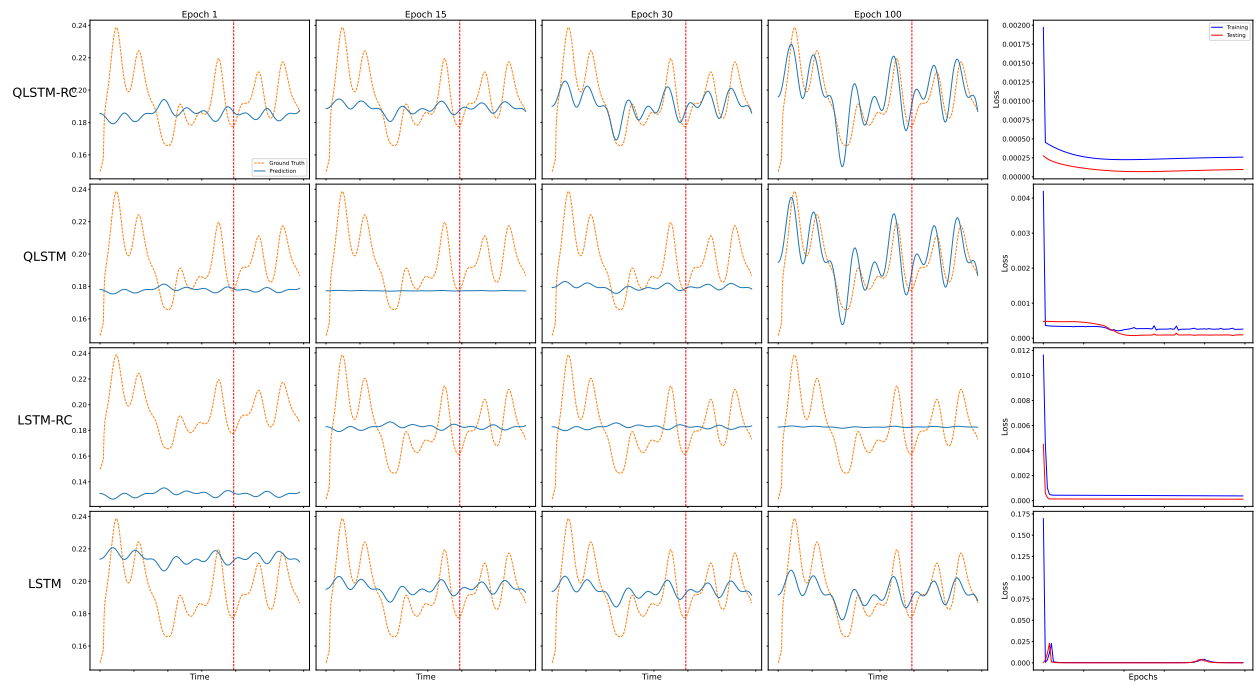


FIG. 21. Learning the NARMA10 with QLSTM-RC.

## ACKNOWLEDGMENTS

The authors would like to thank Constantin Gonciulea and Vanio Markov for constructive and helpful discussions during the development of this paper. The views expressed in this article are those of the authors and do not represent the views of Wells Fargo. This article is for informational purposes only. Nothing contained in this article should be construed as investment advice. Wells Fargo makes no express or implied warranties and expressly disclaims all legal, tax, and accounting implications related to this article.

- 
- [1] A. W. Harrow and A. Montanaro, “Quantum computational supremacy,” *Nature*, vol. 549, no. 7671, pp. 203–209, 2017.
  - [2] M. A. Nielsen and I. Chuang, “Quantum computation and quantum information,” 2002.
  - [3] P. W. Shor, “Algorithms for quantum computation: discrete logarithms and factoring,” in *Proceedings 35th annual symposium on foundations of computer science*, pp. 124–134, Ieee, 1994.
  - [4] L. K. Grover, “A fast quantum mechanical algorithm for database search,” in *Proceedings of the twenty-eighth annual ACM symposium on Theory of computing*, pp. 212–219, 1996.
  - [5] A. Cross, “The ibm q experience and qiskit open-source quantum computing software,” in *APS March meeting abstracts*, vol. 2018, pp. L58–003, 2018.
  - [6] F. Arute, K. Arya, R. Babbush, D. Bacon, J. C. Bardin, R. Barends, R. Biswas, S. Boixo, F. G. Brandao, D. A. Buell, *et al.*, “Quantum supremacy using a programmable superconducting processor,” *Nature*, vol. 574, no. 7779, pp. 505–510, 2019.
  - [7] S. Debnath, N. M. Linke, C. Figgatt, K. A. Landsman, K. Wright, and C. Monroe, “Demonstration of a small programmable quantum computer with atomic qubits,” *Nature*, vol. 536, no. 7614, pp. 63–66, 2016.
  - [8] K. Cho, B. Van Merriënboer, C. Gulcehre, D. Bahdanau, F. Bougares, H. Schwenk, and Y. Bengio, “Learning phrase representations using rnn encoder-decoder for statistical machine translation,” *arXiv preprint arXiv:1406.1078*, 2014.

- [9] I. Sutskever, O. Vinyals, and Q. V. Le, “Sequence to sequence learning with neural networks,” *Advances in neural information processing systems*, vol. 27, 2014.
- [10] A. Graves, A.-r. Mohamed, and G. Hinton, “Speech recognition with deep recurrent neural networks,” in *2013 IEEE international conference on acoustics, speech and signal processing*, pp. 6645–6649, Ieee, 2013.
- [11] A. Graves and N. Jaitly, “Towards end-to-end speech recognition with recurrent neural networks,” in *International conference on machine learning*, pp. 1764–1772, PMLR, 2014.
- [12] H. Sak, A. Senior, K. Rao, and F. Beaufays, “Fast and accurate recurrent neural network acoustic models for speech recognition,” *arXiv preprint arXiv:1507.06947*, 2015.
- [13] H. Sak, A. Senior, and F. Beaufays, “Long short-term memory based recurrent neural network architectures for large vocabulary speech recognition,” *arXiv preprint arXiv:1402.1128*, 2014.
- [14] A. Krizhevsky, I. Sutskever, and G. E. Hinton, “Imagenet classification with deep convolutional neural networks,” in *Advances in neural information processing systems*, pp. 1097–1105, 2012.
- [15] C. Szegedy, W. Liu, Y. Jia, P. Sermanet, S. Reed, D. Anguelov, D. Erhan, V. Vanhoucke, and A. Rabinovich, “Going deeper with convolutions,” in *Proceedings of the IEEE conference on Computer Vision and Pattern Recognition*, pp. 1–9, 2015.
- [16] K. Simonyan and A. Zisserman, “Very deep convolutional networks for large-scale image recognition,” *arXiv preprint arXiv:1409.1556*, 2014.
- [17] Y. LeCun, L. Bottou, Y. Bengio, and P. Haffner, “Gradient-based learning applied to document recognition,” *Proceedings of the IEEE*, vol. 86, no. 11, pp. 2278–2324, 1998.
- [18] K. He, X. Zhang, S. Ren, and J. Sun, “Deep residual learning for image recognition,” in *Proceedings of the IEEE conference on computer vision and pattern recognition*, pp. 770–778, 2016.
- [19] D. Silver, J. Schrittwieser, K. Simonyan, I. Antonoglou, A. Huang, A. Guez, T. Hubert, L. Baker, M. Lai, A. Bolton, *et al.*, “Mastering the game of go without human knowledge,” *nature*, vol. 550, no. 7676, pp. 354–359, 2017.
- [20] D. Silver, A. Huang, C. J. Maddison, A. Guez, L. Sifre, G. Van Den Driessche, J. Schrittwieser, I. Antonoglou, V. Panneershelvam, M. Lanctot, *et al.*, “Mastering the game of go with deep neural networks and tree search,” *nature*, vol. 529, no. 7587, pp. 484–489, 2016.

- [21] V. Mnih, K. Kavukcuoglu, D. Silver, A. A. Rusu, J. Veness, M. G. Bellemare, A. Graves, M. Riedmiller, A. K. Fidjeland, G. Ostrovski, S. Petersen, C. Beattie, A. Sadik, I. Antonoglou, H. King, D. Kumaran, D. Wierstra, S. Legg, and D. Hassabis, “Human-level control through deep reinforcement learning,” *Nature*, vol. 518, pp. 529–533, 2 2015.
- [22] J. Schrittwieser, I. Antonoglou, T. Hubert, K. Simonyan, L. Sifre, S. Schmitt, A. Guez, E. Lockhart, D. Hassabis, T. Graepel, *et al.*, “Mastering atari, go, chess and shogi by planning with a learned model,” *arXiv preprint arXiv:1911.08265*, 2019.
- [23] A. P. Badia, B. Piot, S. Kapturowski, P. Sprechmann, A. Vitvitskyi, D. Guo, and C. Blundell, “Agent57: Outperforming the atari human benchmark,” *arXiv preprint arXiv:2003.13350*, 2020.
- [24] V. Dunjko and H. J. Briegel, “Machine learning & artificial intelligence in the quantum domain: a review of recent progress,” *Reports on Progress in Physics*, vol. 81, no. 7, p. 074001, 2018.
- [25] J. Biamonte, P. Wittek, N. Pancotti, P. Rebentrost, N. Wiebe, and S. Lloyd, “Quantum machine learning,” *Nature*, vol. 549, no. 7671, pp. 195–202, 2017.
- [26] S. Dupond, “A thorough review on the current advance of neural network structures,” *Annual Reviews in Control*, vol. 14, pp. 200–230, 2019.
- [27] O. I. Abiodun, A. Jantan, A. E. Omolara, K. V. Dada, N. A. Mohamed, and H. Arshad, “State-of-the-art in artificial neural network applications: A survey,” *Heliyon*, vol. 4, no. 11, p. e00938, 2018.
- [28] A. Tealab, “Time series forecasting using artificial neural networks methodologies: A systematic review,” *Future Computing and Informatics Journal*, vol. 3, no. 2, pp. 334–340, 2018.
- [29] K. Cho, B. Van Merriënboer, D. Bahdanau, and Y. Bengio, “On the properties of neural machine translation: Encoder-decoder approaches,” *arXiv preprint arXiv:1409.1259*, 2014.
- [30] S. Hochreiter and J. Schmidhuber, “Long short-term memory,” *Neural computation*, vol. 9, no. 8, pp. 1735–1780, 1997.
- [31] J. T. Connor, R. D. Martin, and L. E. Atlas, “Recurrent neural networks and robust time series prediction,” *IEEE transactions on neural networks*, vol. 5, no. 2, pp. 240–254, 1994.
- [32] Y. Hua, Z. Zhao, R. Li, X. Chen, Z. Liu, and H. Zhang, “Deep learning with long short-term memory for time series prediction,” *IEEE Communications Magazine*, vol. 57, no. 6,

- pp. 114–119, 2019.
- [33] J. Bausch, “Recurrent quantum neural networks,” *arXiv preprint arXiv:2006.14619*, 2020.
- [34] Y. Takaki, K. Mitarai, M. Negoro, K. Fujii, and M. Kitagawa, “Learning temporal data with a variational quantum recurrent neural network,” *Physical Review A*, vol. 103, no. 5, p. 052414, 2021.
- [35] S. Y.-C. Chen, S. Yoo, and Y.-L. L. Fang, “Quantum long short-term memory,” in *ICASSP 2022-2022 IEEE International Conference on Acoustics, Speech and Signal Processing (ICASSP)*, pp. 8622–8626, IEEE, 2022.
- [36] M. Cerezo, A. Arrasmith, R. Babbush, S. C. Benjamin, S. Endo, K. Fujii, J. R. McClean, K. Mitarai, X. Yuan, L. Cincio, *et al.*, “Variational quantum algorithms,” *Nature Reviews Physics*, vol. 3, no. 9, pp. 625–644, 2021.
- [37] K. Mitarai, M. Negoro, M. Kitagawa, and K. Fujii, “Quantum circuit learning,” *Physical Review A*, vol. 98, no. 3, p. 032309, 2018.
- [38] M. Schuld, V. Bergholm, C. Gogolin, J. Izaac, and N. Killoran, “Evaluating analytic gradients on quantum hardware,” *Physical Review A*, vol. 99, no. 3, p. 032331, 2019.
- [39] H. Jaeger and H. Haas, “Harnessing nonlinearity: Predicting chaotic systems and saving energy in wireless communication,” *science*, vol. 304, no. 5667, pp. 78–80, 2004.
- [40] H. Jaeger, “The “echo state” approach to analysing and training recurrent neural networks with an erratum note,” *Bonn, Germany: German National Research Center for Information Technology GMD Technical Report*, vol. 148, no. 34, p. 13, 2001.
- [41] G. Tanaka, T. Yamane, J. B. Héroux, R. Nakane, N. Kanazawa, S. Takeda, H. Numata, D. Nakano, and A. Hirose, “Recent advances in physical reservoir computing: A review,” *Neural Networks*, vol. 115, pp. 100–123, 2019.
- [42] B. Krollner, B. J. Vanstone, G. R. Finnie, *et al.*, “Financial time series forecasting with machine learning techniques: a survey.,” in *ESANN*, 2010.
- [43] A. Dingli and K. S. Fournier, “Financial time series forecasting-a deep learning approach,” *International Journal of Machine Learning and Computing*, vol. 7, no. 5, pp. 118–122, 2017.
- [44] S. Hochreiter, “The vanishing gradient problem during learning recurrent neural nets and problem solutions,” *International Journal of Uncertainty, Fuzziness and Knowledge-Based Systems*, vol. 6, no. 02, pp. 107–116, 1998.

- [45] R. Pascanu, T. Mikolov, and Y. Bengio, “On the difficulty of training recurrent neural networks,” in *International conference on machine learning*, pp. 1310–1318, PMLR, 2013.
- [46] R. Miikkulainen, *Reservoir Computing*, pp. 1103–1104. Boston, MA: Springer US, 2017.
- [47] M. C. Caro, H.-Y. Huang, M. Cerezo, K. Sharma, A. Sornborger, L. Cincio, and P. J. Coles, “Generalization in quantum machine learning from few training data,” *Nature communications*, vol. 13, no. 1, pp. 1–11, 2022.
- [48] Y. Du, M.-H. Hsieh, T. Liu, and D. Tao, “The expressive power of parameterized quantum circuits,” *arXiv preprint arXiv:1810.11922*, 2018.
- [49] A. Abbas, D. Sutter, C. Zoufal, A. Lucchi, A. Figalli, and S. Woerner, “The power of quantum neural networks,” *Nature Computational Science*, vol. 1, no. 6, pp. 403–409, 2021.
- [50] A. Pellow-Jarman, I. Sinayskiy, A. Pillay, and F. Petruccione, “A comparison of various classical optimizers for a variational quantum linear solver,” *Quantum Information Processing*, vol. 20, no. 6, pp. 1–14, 2021.
- [51] L. Franken, B. Georgiev, S. Muecke, M. Wolter, N. Piatkowski, and C. Bauckhage, “Gradient-free quantum optimization on nisy devices,” *arXiv preprint arXiv:2012.13453*, 2020.
- [52] A. Kandala, A. Mezzacapo, K. Temme, M. Takita, M. Brink, J. M. Chow, and J. M. Gambetta, “Hardware-efficient variational quantum eigensolver for small molecules and quantum magnets,” *Nature*, vol. 549, no. 7671, pp. 242–246, 2017.
- [53] E. Farhi, J. Goldstone, and S. Gutmann, “A quantum approximate optimization algorithm,” *arXiv preprint arXiv:1411.4028*, 2014.
- [54] J. R. McClean, J. Romero, R. Babbush, and A. Aspuru-Guzik, “The theory of variational hybrid quantum-classical algorithms,” *New Journal of Physics*, vol. 18, no. 2, p. 023023, 2016.
- [55] M. Schuld, A. Bocharov, K. Svore, and N. Wiebe, “Circuit-centric quantum classifiers,” *arXiv preprint arXiv:1804.00633*, 2018.
- [56] V. Havlíček, A. D. Córcoles, K. Temme, A. W. Harrow, A. Kandala, J. M. Chow, and J. M. Gambetta, “Supervised learning with quantum-enhanced feature spaces,” *Nature*, vol. 567, no. 7747, pp. 209–212, 2019.
- [57] E. Farhi and H. Neven, “Classification with quantum neural networks on near term processors,” *arXiv preprint arXiv:1802.06002*, 2018.

- [58] M. Benedetti, E. Lloyd, S. Sack, and M. Fiorentini, “Parameterized quantum circuits as machine learning models,” *Quantum Science and Technology*, vol. 4, no. 4, p. 043001, 2019.
- [59] A. Mari, T. R. Bromley, J. Izaac, M. Schuld, and N. Killoran, “Transfer learning in hybrid classical-quantum neural networks,” *Quantum*, vol. 4, p. 340, 2020.
- [60] Z. Abohashima, M. Elhosen, E. H. Houssein, and W. M. Mohamed, “Classification with quantum machine learning: A survey,” *arXiv preprint arXiv:2006.12270*, 2020.
- [61] P. Easom-McCaldin, A. Bouridane, A. Belatreche, and R. Jiang, “Towards building a facial identification system using quantum machine learning techniques,” *arXiv preprint arXiv:2008.12616*, 2020.
- [62] A. Sarma, R. Chatterjee, K. Gili, and T. Yu, “Quantum unsupervised and supervised learning on superconducting processors,” *arXiv preprint arXiv:1909.04226*, 2019.
- [63] S. A. Stein, B. Baheri, R. M. Tischio, Y. Chen, Y. Mao, Q. Guan, A. Li, and B. Fang, “A hybrid system for learning classical data in quantum states,” *arXiv preprint arXiv:2012.00256*, 2020.
- [64] S. Y.-C. Chen, C.-M. Huang, C.-W. Hsing, and Y.-J. Kao, “Hybrid quantum-classical classifier based on tensor network and variational quantum circuit,” *arXiv preprint arXiv:2011.14651*, 2020.
- [65] S. Y.-C. Chen, T.-C. Wei, C. Zhang, H. Yu, and S. Yoo, “Quantum convolutional neural networks for high energy physics data analysis,” *Physical Review Research*, vol. 4, no. 1, p. 013231, 2022.
- [66] S. L. Wu, J. Chan, W. Guan, S. Sun, A. Wang, C. Zhou, M. Livny, F. Carminati, A. Di Meglio, A. C. Li, *et al.*, “Application of quantum machine learning using the quantum variational classifier method to high energy physics analysis at the lhc on ibm quantum computer simulator and hardware with 10 qubits,” *arXiv preprint arXiv:2012.11560*, 2020.
- [67] S. A. Stein, Y. Mao, B. Baheri, Q. Guan, A. Li, D. Chen, S. Xu, and C. Ding, “Quclassi: A hybrid deep neural network architecture based on quantum state fidelity,” *arXiv preprint arXiv:2103.11307*, 2021.
- [68] S. Y.-C. Chen, T.-C. Wei, C. Zhang, H. Yu, and S. Yoo, “Hybrid quantum-classical graph convolutional network,” *arXiv preprint arXiv:2101.06189*, 2021.
- [69] B. Jaderberg, L. W. Anderson, W. Xie, S. Albanie, M. Kiffner, and D. Jaksch, “Quantum self-supervised learning,” *arXiv preprint arXiv:2103.14653*, 2021.

- [70] D. Mattern, D. Martyniuk, H. Willems, F. Bergmann, and A. Paschke, “Variational quantum neural networks with enhanced image encoding,” *arXiv preprint arXiv:2106.07327*, 2021.
- [71] J. Qi, C.-H. H. Yang, and P.-Y. Chen, “Qtn-vqc: An end-to-end learning framework for quantum neural networks,” *arXiv preprint arXiv:2110.03861*, 2021.
- [72] O. Kyriienko and E. B. Magnusson, “Unsupervised quantum machine learning for fraud detection,” *arXiv preprint arXiv:2208.01203*, 2022.
- [73] W. Li, Z. Lu, and D.-L. Deng, “Quantum neural network classifiers: A tutorial,” *arXiv preprint arXiv:2206.02806*, 2022.
- [74] J. Wu, Z. Tao, and Q. Li, “Scalable quantum neural networks for classification,” *arXiv preprint arXiv:2208.07719*, 2022.
- [75] N. Nguyen and K.-C. Chen, “Bayesian quantum neural networks,” *IEEE Access*, 2022.
- [76] P.-L. Dallaire-Demers and N. Killoran, “Quantum generative adversarial networks,” *Physical Review A*, vol. 98, no. 1, p. 012324, 2018.
- [77] S. A. Stein, B. Baheri, R. M. Tischio, Y. Mao, Q. Guan, A. Li, B. Fang, and S. Xu, “Qugan: A generative adversarial network through quantum states,” *arXiv preprint arXiv:2010.09036*, 2020.
- [78] C. Zoufal, A. Lucchi, and S. Woerner, “Quantum generative adversarial networks for learning and loading random distributions,” *npj Quantum Information*, vol. 5, no. 1, pp. 1–9, 2019.
- [79] H. Situ, Z. He, L. Li, and S. Zheng, “Quantum generative adversarial network for generating discrete data,” *arXiv preprint arXiv:1807.01235*, 2018.
- [80] K. Nakaji and N. Yamamoto, “Quantum semi-supervised generative adversarial network for enhanced data classification,” *arXiv preprint arXiv:2010.13727*, 2020.
- [81] S. Y.-C. Chen, C.-H. H. Yang, J. Qi, P.-Y. Chen, X. Ma, and H.-S. Goan, “Variational quantum circuits for deep reinforcement learning,” *IEEE Access*, vol. 8, pp. 141007–141024, 2020.
- [82] S. Y.-C. Chen, C.-M. Huang, C.-W. Hsing, H.-S. Goan, and Y.-J. Kao, “Variational quantum reinforcement learning via evolutionary optimization,” *Machine Learning: Science and Technology*, vol. 3, no. 1, p. 015025, 2022.
- [83] O. Lockwood and M. Si, “Reinforcement learning with quantum variational circuit,” in *Proceedings of the AAAI Conference on Artificial Intelligence and Interactive Digital Entertainment*

- ment, vol. 16, pp. 245–251, 2020.
- [84] S. Jerbi, L. M. Trenkwalder, H. P. Nautrup, H. J. Briegel, and V. Dunjko, “Quantum enhancements for deep reinforcement learning in large spaces,” *PRX Quantum*, vol. 2, no. 1, p. 010328, 2021.
- [85] C.-C. CHEN, K. SHIBA, M. SOGABE, K. SAKAMOTO, and T. SOGABE, “Hybrid quantum-classical ulam-von neumann linear solver-based quantum dynamic programming algorithm,” *Proceedings of the Annual Conference of JSAI*, vol. JSAI2020, pp. 2K6ES203–2K6ES203, 2020.
- [86] S. Wu, S. Jin, D. Wen, and X. Wang, “Quantum reinforcement learning in continuous action space,” *arXiv preprint arXiv:2012.10711*, 2020.
- [87] A. Skolik, S. Jerbi, and V. Dunjko, “Quantum agents in the gym: a variational quantum algorithm for deep q-learning,” *Quantum*, vol. 6, p. 720, 2022.
- [88] S. Jerbi, C. Gyurik, S. Marshall, H. J. Briegel, and V. Dunjko, “Variational quantum policies for reinforcement learning,” *arXiv preprint arXiv:2103.05577*, 2021.
- [89] J.-Y. Hsiao, Y. Du, W.-Y. Chiang, M.-H. Hsieh, and H.-S. Goan, “Unentangled quantum reinforcement learning agents in the openai gym,” *arXiv preprint arXiv:2203.14348*, 2022.
- [90] W. J. Yun, Y. Kwak, J. P. Kim, H. Cho, S. Jung, J. Park, and J. Kim, “Quantum multi-agent reinforcement learning via variational quantum circuit design,” *arXiv preprint arXiv:2203.10443*, 2022.
- [91] A. Sequeira, L. P. Santos, and L. S. Barbosa, “Variational quantum policy gradients with an application to quantum control,” *arXiv preprint arXiv:2203.10591*, 2022.
- [92] D. Heimann, H. Hohenfeld, F. Wiebe, and F. Kirchner, “Quantum deep reinforcement learning for robot navigation tasks,” *arXiv preprint arXiv:2202.12180*, 2022.
- [93] M. Schenk, E. F. Combarro, M. Grossi, V. Kain, K. S. B. Li, M.-M. Popa, and S. Vallecorsa, “Hybrid actor-critic algorithm for quantum reinforcement learning at cern beam lines,” *arXiv preprint arXiv:2209.11044*, 2022.
- [94] S. Y.-C. Chen, “Quantum deep recurrent reinforcement learning,” *arXiv preprint arXiv:2210.14876*, 2022.
- [95] C.-H. H. Yang, J. Qi, S. Y.-C. Chen, P.-Y. Chen, S. M. Siniscalchi, X. Ma, and C.-H. Lee, “Decentralizing feature extraction with quantum convolutional neural network for automatic speech recognition,” in *ICASSP 2021-2021 IEEE International Conference on Acoustics,*

- Speech and Signal Processing (ICASSP)*, pp. 6523–6527, IEEE, 2021.
- [96] J. Qi and J. Tejedor, “Classical-to-quantum transfer learning for spoken command recognition based on quantum neural networks,” in *ICASSP 2022-2022 IEEE International Conference on Acoustics, Speech and Signal Processing (ICASSP)*, pp. 8627–8631, IEEE, 2022.
- [97] C.-H. H. Yang, J. Qi, S. Y.-C. Chen, Y. Tsao, and P.-Y. Chen, “When bert meets quantum temporal convolution learning for text classification in heterogeneous computing,” in *ICASSP 2022-2022 IEEE International Conference on Acoustics, Speech and Signal Processing (ICASSP)*, pp. 8602–8606, IEEE, 2022.
- [98] R. Di Sipio, J.-H. Huang, S. Y.-C. Chen, S. Mangini, and M. Worring, “The dawn of quantum natural language processing,” in *ICASSP 2022-2022 IEEE International Conference on Acoustics, Speech and Signal Processing (ICASSP)*, pp. 8612–8616, IEEE, 2022.
- [99] S. Lloyd, M. Schuld, A. Ijaz, J. Izaac, and N. Killoran, “Quantum embeddings for machine learning,” *arXiv preprint arXiv:2001.03622*, 2020.
- [100] N. A. Nghiem, S. Y.-C. Chen, and T.-C. Wei, “Unified framework for quantum classification,” *Physical Review Research*, vol. 3, no. 3, p. 033056, 2021.
- [101] S. Y.-C. Chen and S. Yoo, “Federated quantum machine learning,” *Entropy*, vol. 23, no. 4, p. 460, 2021.
- [102] M. Chehimi and W. Saad, “Quantum federated learning with quantum data,” in *ICASSP 2022-2022 IEEE International Conference on Acoustics, Speech and Signal Processing (ICASSP)*, pp. 8617–8621, IEEE, 2022.
- [103] S. Sim, P. D. Johnson, and A. Aspuru-Guzik, “Expressibility and entangling capability of parameterized quantum circuits for hybrid quantum-classical algorithms,” *Advanced Quantum Technologies*, vol. 2, no. 12, p. 1900070, 2019.
- [104] T. Lanting, A. J. Przybysz, A. Y. Smirnov, F. M. Spedalieri, M. H. Amin, A. J. Berkley, R. Harris, F. Altomare, S. Boixo, P. Bunyk, *et al.*, “Entanglement in a quantum annealing processor,” *Physical Review X*, vol. 4, no. 2, p. 021041, 2014.
- [105] K. Hornik, M. Stinchcombe, H. White, *et al.*, “Multilayer feedforward networks are universal approximators,” *Neural networks*, vol. 2, no. 5, pp. 359–366, 1989.
- [106] V. Bergholm, J. Izaac, M. Schuld, C. Gogolin, M. S. Alam, S. Ahmed, J. M. Arrazola, C. Blank, A. Delgado, S. Jahangiri, *et al.*, “Pennylane: Automatic differentiation of hybrid quantum-classical computations,” *arXiv preprint arXiv:1811.04968*, 2018.

- [107] H. Salehinejad, S. Sankar, J. Barfett, E. Colak, and S. Valaee, “Recent advances in recurrent neural networks,” *arXiv preprint arXiv:1801.01078*, 2017.
- [108] M. Lukoševičius and H. Jaeger, “Reservoir computing approaches to recurrent neural network training,” *Computer Science Review*, vol. 3, no. 3, pp. 127–149, 2009.
- [109] R. LaRose and B. Coyle, “Robust data encodings for quantum classifiers,” *Physical Review A*, vol. 102, no. 3, p. 032420, 2020.
- [110] A. Paszke, S. Gross, F. Massa, A. Lerer, J. Bradbury, G. Chanan, T. Killeen, Z. Lin, N. Gimelshein, L. Antiga, *et al.*, “Pytorch: An imperative style, high-performance deep learning library,” *Advances in neural information processing systems*, vol. 32, 2019.
- [111] T. Tieleman and G. Hinton, “Lecture 6.5—RmsProp: Divide the gradient by a running average of its recent magnitude.” COURSERA: Neural Networks for Machine Learning, 2012.
- [112] K. Georgopoulos, C. Emary, and P. Zuliani, “Modeling and simulating the noisy behavior of near-term quantum computers,” *Physical Review A*, vol. 104, no. 6, p. 062432, 2021.
- [113] M. L. Dahlhauser and T. S. Humble, “Modeling noisy quantum circuits using experimental characterization,” *Physical Review A*, vol. 103, no. 4, p. 042603, 2021.
- [114] A. Atiya and A. Parlos, “New results on recurrent network training: unifying the algorithms and accelerating convergence,” *IEEE transactions on neural networks*, vol. 11, no. 3, pp. 697–709, 2000.
- [115] A. Goudarzi, P. Banda, M. R. Lakin, C. Teuscher, and D. Stefanovic, “A comparative study of reservoir computing for temporal signal processing,” 2014.
- [116] Y. Suzuki, Q. Gao, K. C. Pradel, K. Yasuoka, and N. Yamamoto, “Natural quantum reservoir computing for temporal information processing,” *Scientific reports*, vol. 12, no. 1, pp. 1–15, 2022.
- [117] J. Preskill, “Quantum computing in the nisq era and beyond,” *Quantum*, vol. 2, p. 79, 2018.
- [118] C.-H. H. Yang, Y.-Y. Tsai, and P.-Y. Chen, “Voice2series: Reprogramming acoustic models for time series classification,” in *International Conference on Machine Learning*, pp. 11808–11819, PMLR, 2021.
- [119] D. J. Egger, C. Gambella, J. Marecek, S. McFaddin, M. Mevissen, R. Raymond, A. Simonetto, S. Woerner, and E. Yndurain, “Quantum computing for finance: State-of-the-art and future prospects,” *IEEE Transactions on Quantum Engineering*, vol. 1, pp. 1–24, 2020.